Modeling and Control of a Solenoid Actuator with Application to Electric Vehicle Transmissions

Rana Tahmasebi

Department of Electrical & Computer Engineering
McGill University
Montreal, Canada

November 2014

A thesis submitted to McGill University in partial fulfillment of the requirements for the degree of Master in Engineering.

Abstract

Solenoid actuators are one of the solutions for efficient gear shifting in electric vehicles (EVs). In this thesis, a new approach for modeling solenoid actuators is proposed. Moreover, a robust force controller for the actuators is designed using the proposed modeling approach. Such control problems are of interest in the study of gear shifting control in EVs equipped with an automated manual transmission. In this thesis, experimental system identification along with the finite element method (FEM) are employed to model the dynamic behavior of the solenoid actuators as well as the system uncertainties. Using experimental system identification, a dynamic model of the actuators is obtained and a nonlinear algebraic model of the electromagnetic force versus current and air gap is proposed. Using the properties of the magnetic materials and the geometry of the actuator, an FEM analysis is performed using MagNet® —a software developed by Infolytica— to obtain the dynamics of the nominal system and verify the system identification results. Considering the inherent uncertainties of the physical parameters involved in the actuation system as well as the measurement errors, an uncertainty analysis is performed to obtain the dynamic uncertainty model of the solenoid system. Moreover, considering the application of these actuators in the gear shifting process, the closed-loop performance objectives are defined with respect to the desired gear shifting quality. Knowing both the nominal system model and the uncertainty model, an H_∞ robust controller is designed. The performance of the resulting robust closed-loop control system is examined for the nominal and perturbed systems and is shown to satisfy the objectives.

Résumé

L'utilisation d'actionneurs à solénoïde est l'une des solutions pour effectuer des changements de vitesses efficaces dans les véhicules électriques. Dans cette thèse, une nouvelle approche est proposée pour modéliser les actionneurs à solénoïde. De plus, un contrôleur de force robuste pour ces actionneurs est conçu en utilisant l'approche de modélisation proposée. De tels problèmes de contrôle sont pertinents dans l'étude des changements de vitesse pour les véhicules électriques équipés d'une transmission manuelle automatisée. Dans cette thèse, identification de système expérimentale ainsi que la méthode des éléments finis (MEF) sont utilisées pour modéliser le comportement dynamique des actionneurs à solénoïde ainsi que les incertitudes du système. Un modèle dynamique des actionneurs est obtenu grâce à identification de système expérimentale et un modèle algébrique non-linéaire de la force électromagnétique par rapport au courant et à l'entrefer est proposé. En utilisant la géométrie de l'actionneur ainsi que les propriétés des matériaux magnétiques, une analyse MEF est effectuée en utilisant MagNet® —un logiciel développé par Infolytica— dans le but d'obtenir la dynamique du système et de vérifier les résultats de identification de système. Compte tenu des incertitudes inhérentes aux paramètres physiques intervenant dans le système d'actionnement ainsi que lors des erreurs de mesure, une analyse d'incertitude est effectuée dans le but d'obtenir un modèle d'incertitude dynamique du système électro-aimant. En considérant l'application de ces actionneurs dans le processus de changement de vitesse, les objectifs de performance sont définis par rapport à la qualité de changement de vitesse désirée. En connaissant tant le modèle du système nominal que le modèle d'incertitude, un contrôleur H_∞ est conçu. Les performances du système de contrôle en boucle fermée sont étudiées autant pour le système nominal que pour le système perturbé et les objectifs sont atteints.

The secrets eternal neither you know nor I

And answers to the riddle neither you know nor I

Behind the veil there is much talk about us, why

When the veil falls, neither you remain nor I.

Khayyam

Dedication

To my parents, Zohreh and Amir, and my brother, Shahab for their unconditional love and support, and

to my husband, Ali who has been a great source of motivation and inspiration for me

Acknowledgments

My deepest recognition goes to my supervisor, Professor Benoit Boulet for his unconditional help, excellent knowledge of the field and providing the whole team with an excellent atmosphere for doing research. I have been extremely lucky to have a supervisor who cared so much about my work, and who responded to my questions and queries so promptly. He is the most knowledgeable supervisor that I have ever come across. There are no words to express my gratitude for all of the help and support he offered to me during my studies at McGill University. One simply could not wish for a more supportive supervisor.

I wish to thank the Ph.D. candidate at CIM lab, Mr. Hossein Vahid Alizadeh for his good advice and support in developing bright ideas regarding this research, for which I am extremely grateful. I would like to thank CIM Ph.D. candidate, Mr. Mir Saman Rahimi Mousavi for helping in building the experimental setup and in acquiring data from the experimental tests. I thank the research engineer in APC project, Dr. Ying Xuan Duan, for her kindness, friendship and support. I praise the enormous amount of help from the APC project members at McGill University. Thank you Dr. Tao Wang, Sajid Hussain, Ali Pakniyat, Reza Lotfalian, Maria Alkadri, and Dr. Tanvir Rahman.

This work would have not been completed without the financial support from NSERC, Infolytica, TM4, and Linamar. Also, the author acknowledges the support from the Infoltica company for granting the access to the MagNet software license and providing support in using this software.

Contents

List of Figures

List of Tables

Chapter 1

Introduction

1.1 Background

It may seem at first that Electric Vehicles (EVs) are a recent innovation to reduce the air pollution produced by internal combustion engine vehicles (ICEVs). However, EVs were invented approximately 50 years before the appearance of ICEVs. It is interesting to know that the first vehicle with the maximum speed of over 100 km/h, which was built in 1899 and named "jamais contente" (never satisfied), was an EV [1].

It is not clear when the first EV was invented [2]. In 1828, a Hungarian inventor, Ányos Jedlik designed and built the first electro-motor to be used in an electric car. Then, Robert Anderson from Scotland, invented a carriage driven by an electric motor. In 1840, the idea of using rails as the conductors of the electricity was patented. Even though, the early EVs were in small scales, in 1842, more practical ones were invented by Thomas Davenport and Robert Davidson. They both used non-rechargeable batteries to feed EVs electrically [2].

As better energy storage options were introduced, EVs became more popular in transportation services. By 1900, EVs were commercialized very successfully and many Euro-

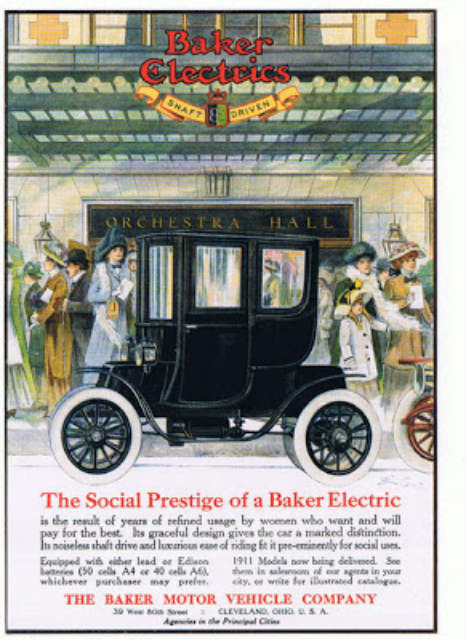

Figure 1.1 Baker Electric EV

pean and American companies were prosperous in this field of industry. In Fig. 1.1, an EV manufactured by Baker Electric Company can be seen.

By 1930s, EVs drastically disappeared from the automotive industry due to the following reasons [2]:

- the road systems were improved and the cities were connected via roads. This led to the manufacture of the vehicles which were able to drive longer distances than EVs,
- the discovery of new oil reservoirs contributed to the decline of gasoline prices and this was a key factor in selecting fossil fuels as the primary source of energy for the vehicle propulsion,
- the ICEVs were more affordable than the conventional EVs.

Even though EVs were not the preferable option in comparison to ICEVs by 1930s, some vehicles such as electric trains were still in use. These trains were mostly used in coal mines, where oxygen would be reserved for other purposes rather than the one consumed

by fossil fuel motors. The newly built ICEVs had lower cost and could go to higher speeds compared to the EVs. All these factors contributed in making ICEVs the most popular type of vehicles until today.

After being forgotten for several decades in the automotive industry, EVs found their way back to the market. In 1970s, increased concerns over environmental preservation and conservation of non-renewable energy resources attracted more attentions toward EVs [3]. By that time, the automotive industry concerns were merely the vehicle cost and speed. However, since the transportation sector was one of the biggest contributers to the emission of green house gases, reduction of emissions from ICEVs became one of the main incentives for reconsidering EVs. Subsequently, attention was devoted to electricity as an alternative source of energy for vehicle propulsion rather than fossil fuel energy.

The electricity consumed by EVs can be generated from a variety of resources including non-renewable energy resources such as nuclear energy and even fossil fuel energy resources as well as renewable resources such as wind and solar energy. The total amount of green-house gas emitted (known as carbon footprint [4]) by an EV depends on the fuel and the method used for the generation of the electricity.

Electricity consumed by an EV can be stored on board in various forms of energies such as chemical energy in batteries, kinetic energy of flywheels, and static energy of super capacitors. These forms of energy would be converted to the electrical energy when needed. Improvement of EVs' efficiency is the topic of recent research, for example, [5] points out the key aspects for management of lithium-ion battery in EVs.

In addition to focusing on EVs as an alternative to ICEVs, in order to decrease the emission of pollutant to the environment, automotive companies started to improve the efficiency of each component in their vehicles. Although, the fuel consumption and gas emission of a vehicle depends on the efficiency of many components, the performance of

the powertrain of a vehicle plays a significant role in defining the efficiency [6]. The main components of the powertrain are engine and transmission system. The performance of the transmission system is the decisive factor in the vehicle's performance [7]. It has been shown that in order to improve the efficiency of a powertrain, it is more cost effective to improve the transmission system efficiency rather than the engine efficiency [8].

1.2 Transmission Systems

A transmission system is an assembly of speed adapting gears and the drive shaft that makes the connection between motor and wheels. When the driver starts, stops, or even drives slowly, there is a significant difference between the speed of the motor and the wheels. The job of a transmission system is to adapt the wheels' speed to the engine's speed using the speed changing gears. Therefore, the engine's torque is transferred to the wheels through the transmission system. There are various types of transmission systems with different applications. In [9], the appropriate transmission systems for the specific applications in various driveline configurations are investigated.

Each transmission system has its own advantages and disadvantages. Selecting an appropriate type of transmission system for EVs is of significant importance. Manual transmission is a common type of transmission system out of north America. Automatic transmission (AT) and automated manual transmission (AMT) are two well-known types of multi-speed transmission systems for ICEVs. AT and AMT can be used in EVs to enhance the performance of the electric drivetrain by providing an appropriate number of gear ratios. Each of these transmission systems are briefly introduced in the following sections.

1.2.1 Manual Transmission

Manual transmission is a well-known type of transmission system employed in motor vehicles. In this type of transmission systems, gear shifting is executed mainly by means of flywheel and pressure plate, clutch, and gears. Flywheel is attached to the engine via a crankshaft from one side, and from the other side it is connected to the clutch. The job of the pressure plate is to fix the clutch firmly to the flywheel in order to ensure that the energy generated in engine is transmitted to the transmission system via the clutch, whenever needed. When the clutch is engaged, it simplifies the connection between the transmission system and the gears. At the same time as the driver is depressing the clutch pedal, the clutch disengages and this will cause the gear shifting procedure to proceed safely.

In order to be able to drive a vehicle equipped with manual transmission, the driver needs to know some skills in gear shifting. This would not make driving a pleasant experience, especially for the ones who have difficulty in changing gears. Although, the manual transmission does not provide ease of driving, it is counted as the transmission system with the highest efficiency of %96.2 [10]. In this type of transmission, lubricant is splashed to keep the transmission internals lubricated. A portion of losses in a vehicle equipped with manual transmission is produced by lubricant churning. Furthermore, seal friction and gear mesh losses are considered as additional sources of losses [11].

In Fig. 1.2, a schematic of a manual transmission system is illustrated. The main components of the manual transmission system such as flywheel (1), clutch (2), and gears (3) can be seen in this figure.

Figure 1.2 Manual transmission components: flywheel (1), clutch (2), and gears (3) [12]

1.2.2 Automatic Transmission

Although, manual transmission is a very efficient transmission system, it does not provide comfort to the driver. To improve the driving experience, automatic transmission (AT) is introduced by the automotive industry. In ATs, changing the prefixed gear ratios is accomplished automatically while the vehicle is moving. In this type of transmission, there is no need for the driver to change the gear ratios manually.

AT operates using a hydraulic actuator, a torque converter (fluid coupling) and some planetary gear sets to build specific gear ratios. The vehicle's motor is hydraulically connected to the gear box by the torque converter. To transfer the motor torque to the transmission system, the torque converter acts very similar to the automatic clutch. Also,

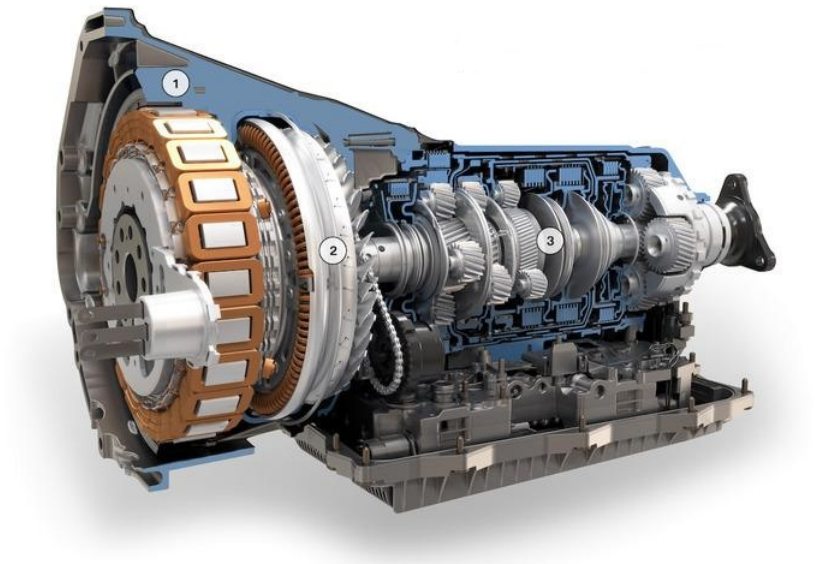

Figure 1.3 Electric motor (1), hydraulic torque converter (2), and 8-speed automatic transmission (3) cutaway in an automatic transmission [13]

it allows the motor to remain idle when the driver stops the vehicle while in gear. A picture of the automatic transmission is shown in Fig. 1.3. In this figure, components such as the vehicle's motor (1), the hydraulic torque converter with lock up clutch (2), and the 8-speed automatic transmission (3) are illustrated.

Even though, ease of driving is an advantage of ATs, they are less efficient than conventional manual transmissions. Viscous and pumping losses in the torque converters and hydraulic actuators are the main factors of the low efficiency of ATs. Moreover, the continuous operation of hydraulic pumps in order to provide the sufficient energy for actuation, clutch cooling, and lubrication of the bearing and the clutch contributes to lower the efficiency of ATs. The overall efficiency of vehicles equipped with ATs are 86.3% [6, 7, 11].

1.2.3 Automated Manual Transmission

Automated manual transmission (AMT) systems were developed to take advantage of benefits of both manual transmissions and ATs. In order to develop an AMT system, actuators are added to a manual transmission system for the purpose of providing an appropriate number of gear ratios and enabling the control of the friction clutch. The transmission control unit is responsible for the control of gear shifting process.

The process of the gear ratio shifting in AMTs is different from ATs. Since changing gears is not done automatically in this type of transmission, it is similar to the manual transmission working principle, except the fact that changing gears is facilitated by means of some electric devices. These electric devices such as sensors, processors and actuators replace the clutch pedal, utilized by the driver in manual transmission, to execute the gear shifting task. In this type of transmission, the friction clutch is depressed by the actuator when the actuator is activated. The actuator is operated when the gear shifting command is received from the transmission control unit or the driver. Then, the required force for gear changing is produced and exerted on the friction clutch. This force is then transferred to the synchronizer which is responsible for smooth engagement of the gears.

The reason for developing this type of transmission system is that the electric equipment reaction is more precise and less faulty than a human reaction. The idea is to have a complete and effective clutch operation using electric equipment when having drivers with different skill levels in gear shifting.

As mentioned earlier, AMT combines the advantages of the manual and automatic transmissions. This transmission system is more fuel and cost efficient than ATs (it has the same efficiency as manual transmissions [14]). From the convenience stand point, AMTs are the preferred options in comparison with manual transmissions. Overall, owing to the high

efficiency and convenience of AMTs, they are the preferred option for EVs in comparison with ATs and manual transmissions. Also, from the transmission manufacturing point of view, it is very easy to switch the vehicle production line from manual transmission to AMTs. In order to transform a manual transmission system to AMT, it is only required to install clutch and transmission actuators and a transmission control unit, which is basically the control module part, on the assembly line.

There is a fast-growing interest toward AMTs. A survey, which was taken on six AMT vehicles in Europe, reported in [15], has discussed the factors to improve the gear shifting quality in this type of transmission. In [14], a non-linear model of an AMT actuated with electro-hydraulic actuator is developed and the validity of the model is confirmed by performing experimental tests on a commercial car.

1.3 Literature Review

In this section, a detailed literature review will be presented. The literature review will focus on the following topics:

1. Common types of the actuators used in the gear shifting system
2. Actuator modeling
3. Actuator control

Each topic is elaborated in a subsection.

1.3.1 Actuator Selection

An actuator is a controllable device that converts one form of energy to motion. Depending on the principles that an actuator is working on, the primary form of energy could

be electric, hydraulic, pneumatic, or even rotary mechanical [16]. Actuators are classified based on the form of energy they convert, such as electromagnetic, electrohydraulic, *etc* [17], [18].

Selection of the appropriate type of actuator for one specific purpose may seem difficult. To select the right actuator which can meet the desired requirements in each task, the following information is required:

- the type and the corresponding characteristics of each type of actuator,
- the form of energy that is available as the input for the actuator,
- and, if applicable, a means to convert the available source of energy to the one compatible with the actuator input.

Actuators are selected depending on demanded performance and desirable characteristics required by the user. For example, in some applications high forces are required and therefore, an actuator with high actuation forces must be selected regardless of the stroke it can provide. The performance attributes of different actuators are presented in Fig. 1.4. In this figure, the dashed diagonal line is separating the actuators with the work capacity of more than 0.1 Nm from the ones with less work capacity.

In Fig. 1.4, it can be observed that each actuator can provide a certain range of force and stroke characteristics. If the force or stroke of the actuator is the main concern of the user, this figure could help the user to choose the right type of actuator. However, when the maximum working frequency and the mass of an actuator are concerns of the user, Fig. 1.5 can be of help for selection of the right type of actuators. In this figure, the operating area of different actuators versus maximum working frequency and the actuator's weight is illustrated. When a user has a clear description of what characteristics are required, the actuator can be easily selected.

Looking at Fig. 1.4 and Fig. 1.5 reveals that magnetostrictive and piezoelectric actuators

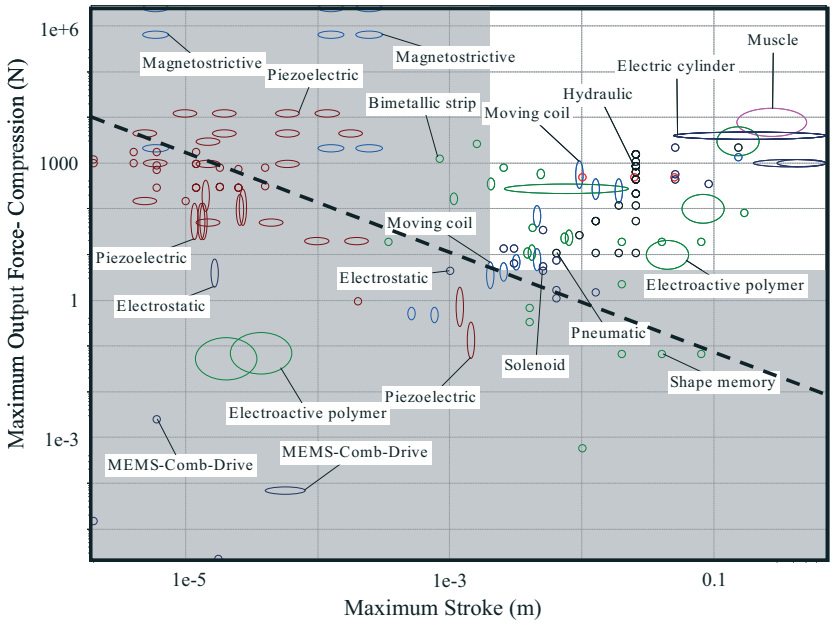

Figure 1.4 A comparison of maximum output force versus maximum stroke for different actuators [18]

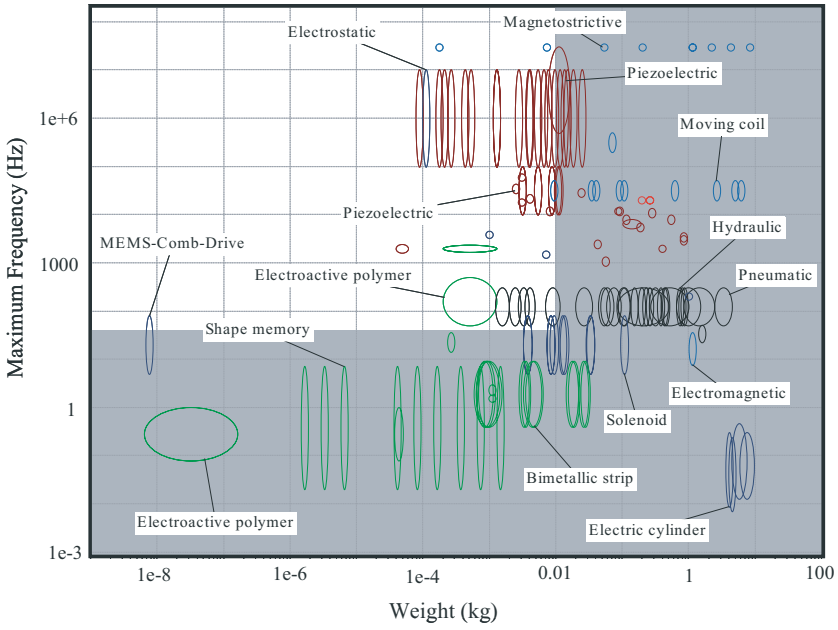

Figure 1.5 A comparison of maximum working frequency versus weight for different actuators [18]

could provide high force density and fast responses while they are not good for long stroke applications. On the other hand, hydraulic and electric cylinder actuators are capable of providing long strokes and high forces, while their response time is not very fast. Therefore, in selection of actuators a trade-off between the performance objectives is required. The user needs to identify the critical and non-critical performance characteristics of the task in order to select the right type of actuator.

1.3.1.1 Actuator Application in Automotive Industry

Actuators play a significant role in simplifying tasks in various fields of industry. Actuators have been employed in the automotive industry to fulfill various tasks in different vehicle components. Considering the capability of actuators to provide vast performance characteristics, they have been employed in different transmission systems. The actuators that are used in this field of industry are mostly hydraulic, electrohydraulic, and electromechanical actuators.

In the following sections, most of the actuators used in transmission systems are introduced and their advantages and disadvantages are discussed. Despite the fact that some of the actuators are not very efficient, they are still in use in transmission systems.

1.3.1.2 Hydraulic Actuators

Pure hydraulic actuators have been employed in ATs due to the high force density that they can provide. However, they have some disadvantages that have made automotive industry experts think about alternatives to hydraulic actuators. Some of these disadvantages are listed below.

- Hydraulic actuators have low efficiency due to the presence of parasitic losses similar to the one in ATs [19].

- Hydraulic actuators are complex, because there are a number of solenoid valves employed in such actuators to transfer the hydraulic pressure to where the force should be exerted [11].
- The hydraulic fluid can leak and therefore, hydraulic actuators require regular maintenance.

Despite the above-mentioned disadvantages of this type of actuators, hydraulic actuators are still in use for gear control in transmission systems. This is because they can provide high forces. Moreover, the hydraulic pumps of these actuators can be mounted away from the actuation point, which is an advantage for the transmission systems employing such type of actuator.

1.3.1.3 Electrohydaulic Actuators

Electrohydaulic actuators are equipped with an electric motor, which recharges the hydraulic accumulator using a pump. The advantage they offer is that they do not constantly consume power (unlike hydraulic actuators). The electrical power is only used periodically to recharge the accumulator [14]. Even though the power consumption of this type of actuators is significantly lower, they mostly have disadvantages similar to the hydraulic actuators in terms of complexity and inefficiency. In order to improve their efficiency, higher flow rates should be produced which consequently requires larger components such as pump, valves, etc. This will lead to the increases in the overall costs.

1.3.1.4 Electromechanical Actuators

Electromechanical actuators have recently become the new option for transmission applications specially in AMTs and dual clutch transmissions (DCTs). They are more efficient and less complex than hydraulic and electrohydraulic actuators. Therefore, they are con-

sidered as alternatives to the old actuators in automotive industry [19].

Electromagnetic actuators are considered among the family of electromechanical actuators. Electromagnetic actuators use the magnetic fields as the medium to convert electrical energy to mechanical energy. Solenoid actuators use the same principle to generate electromagnetic force. To better understand how force is generated in solenoid actuators, it is important to understand the core principles in electromagnetic force generation.

1.3.1.5 Solenoid Actuators

Solenoid actuators provides numerous advantages such as having high power density in a limited stroke, low cost, reduced complexity, and fast switching. This type of actuators are the actuator of choice in industry [20–24]. They are widely used in various fields of industry for diverse applications, such as

- drug delivery [25],
- diesel vehicle fuel injection systems [26],
- antilock braking systems [27] and
- robotics [28].

Considering the advantages of solenoid actuators as well as accessibility of electricity in EVs, in this thesis we suggest the use of solenoid actuators in EVs' transmission systems. In Chapter 2, we provide a detailed feasibility analysis for this suggestion.

Given the wide use of solenoid actuators in different areas, a vast literature exists on the modeling of these actuators. In the next section, we provide a literature review on the modeling approaches of solenoid actuators.

1.3.2 Solenoid Actuator Modeling

In the field of control systems, a dynamic system should be modeled mathematically. The mathematical model represents the characteristics of the dynamic system and its relationships by sets of equations. This model provides the necessary requirement for controlling the dynamic system [29].

From a modeling point of view, abundant studies have been conducted on solenoid actuator modeling. Most notably, [24] is a valuable work with regard to the modeling technique. This paper presents a nonlinear dynamic model of a proportional solenoid valve actuator. The proportional solenoid valve is divided into two parts, solenoid valve and the spool assembly. The solenoid valve is modeled as a resistive-inductive circuit. The spool is modeled as a mechanical spring-mass-damper system. The model proposed in this paper takes the magnetic saturation and hysteresis effects into account. To verify the accuracy of the model, experimental results are compared with the simulation results. Although this paper does not model a solenoid actuator explicitly, the equations used in this work are the same as the equations governing solenoid actuators.

A simplified model of a solenoid in valve applications is suggested in [30]. In this study, it has been assumed that the actuator behaves as a linear first-order lag transfer function. The drawback of this modeling approach is that it does not consider the effects of hysteresis and saturation of magnetic material.

In another attempt to describe the magnetic characteristics, the study in [31] is conducted to predict the flux patterns within the solenoid based on the results from FEM analysis. This approach is used to describe the skin effect on the time lag flux. Also, a description of the magnetization process in transient state is obtained using this approach. The electromagnetic force and other performance characteristics are determined using the

transient magnetization. This approach to the modeling is accurate, even though it is not successful in providing a model for control design purposes.

In [23], the author developed a solution to increase the stroke of a solenoid actuator by augmenting two oscillating springs which are controlled electromagnetically. In this paper, a mathematical model is introduced using finite element analysis. The dynamic model of motion is integrated in this model. Furthermore, experimental tests are carried out to verify the mathematical model. Finally, it has been concluded that this approach is successful in increasing the stroke of solenoid actuators because it requires less energy for providing long stroke and fast response.

In [32], the authors analyzed the electromagnetic control valve behavior under the perturbation of a magnetic field. In this study, a numerical model of the actuator is achieved by a non-linear 2D finite element analysis. Experimental tests are performed under the same perturbations and at the end, the numerical and experimental modelings have been compared.

In [33], an optimized geometry of a constant force solenoid actuator is designed and compared to the original one based on an FEM analysis. In this paper, the solenoid is designed to provide constant force values independent of the plunger position, which is the desired feature in fluid flow control. Also, a pattern for force distribution around the plunger is determined. The forces of both proposed and original actuators were measured and compared.

1.3.3 Solenoid Actuator Control

Closed-loop control of solenoid actuators is a topic that has been extensively studied given the diverse applications of this type of actuators. In [34], a safe seating (with low range velocities such as 0.1 m/s) position control method is proposed. This method is

only based on the observation of the electrical signals. This control approach has removed the acoustical noises and increased the actuator's life time. Also, the system complexity is reduced using this method. The closed-loop system has been tested on a combustion test engine and has met the desirable objectives under cylinder pressure and input voltage variations.

In [35], a novel position estimation method is presented which is based on the incremental inductance of the solenoid. The inductance is obtained from the derivative of the current rise which is measured by a current rise measurement system. Position is then interpolated using a look-up table of incremental inductance, current, and position. The method's applicability is verified by an industrial solenoid valve.

A nonlinear sensorless sliding mode estimation method is proposed in [36]. In this paper, current measurement is used for the solenoid actuator's position and speed estimation. Moreover, hysteresis and saturation effects are neglected and their impacts are compensated in the robust control design. Also, a closed-loop nonlinear position controller is developed using the position estimation from the estimation algorithm proposed and is experimentally tested.

In [37] another position estimation method without any position measurement is suggested. In this paper, position is estimated based on the flux analysis. The flux is obtained by the secondary coil voltage integration which is added at each electromagnet. By this method, the flux and plunger position are accessible for the position closed-loop control purpose. The method is implemented and its validity is confirmed.

1.4 Thesis Contribution

The following results of this research are the main contributions of the author to the advancement of knowledge:

a) The use of solenoid actuators for the gear shifting task of EVs equipped with AMT is proposed.

b) To ensure that solenoid actuators can fulfill the proposed task, a detailed feasibility analysis is presented.

c) A detailed modeling of a solenoid actuator based on three different approaches, namely, (i) theoretical, (ii) numerical (FEM), and (iii) experimental is presented.

d) Having the actuator's geometry and the magnetic properties of the actuator's material, the actuator is modeled in FEM environment. The actuator's steady state and transient state response is achieved using FEM.

e) In order to verify the results from FEM analysis, experimental tests are carried out to model the dynamic and steady state behavior of the actuator. Building the experimental setup and acquiring data from the experimental tests are accomplished with the help of Mr. Hossein Vahid Alizadeh and Mr. Mir Saman Rahimi Mousavi, PhD. candidates in CIM.

f) Using experimental tests, the dynamic and steady state impact of air gap spacer existence in a solenoid actuator is investigated.

g) The sources of uncertainty involved in the modeling of the actuator are identified.

h) A new configuration for the control of the force of the actuator is suggested which transform the force control problem to the current control problem.

i) Considering the presence of uncertainties, a robust controller is designed using the H_∞

optimal control method. The goal of the controller is to ensure that the closed-loop system is robustly stable to all uncertainties.

j) The satisfactory controller performance is validated using simulation of the closed-loop system under presence of uncertain conditions.

1.5 Thesis Outline

The succeeding chapters are composed as follows:

- In the beginning of Chapter 2, we analyze the required force for gear shifting in an AMT. Then, a feasibility analysis is performed to determine if solenoid actuators are able to meet the required characteristics of a gear shifting task in an AMT. Furthermore, a suitable solenoid actuator is selected. In the remainder of the chapter, three different approaches for the modeling of the selected actuator are presented. The first approach is the simplified theoretical approach. The second approach is modeling of the actuator using FEM. The FEM analysis is performed by MagNet®—a software developed by Infolytica. FEM is a very accurate tool for solving sophisticated Maxwell's equations. The experimental approach is introduced as a complementary approach to the FEM modeling. An experimental setup is built for this purpose. Finally, an algebraic non-linear model of force versus current and air gap length as well as several uncertain linear dynamic models of current versus voltage are proposed.
- In Chapter 3, considering the parametric uncertainties involved in the modeling of the actuator, an uncertainty analysis is performed. Since models with uncertainties should satisfy robustness and performance objectives, the design of a robust force control system is necessary. The controller should be designed so that the closed-loop system perfectly operates under uncertain circumstances. In the remainder of this

chapter, the closed-loop force controller is designed using the H_∞ optimal control method, based on the uncertainty analysis performed beforehand. A new closed-loop configuration for reducing the problem complexity is suggested. The effectiveness of the controller is evaluated by simulation to ensure that the proposed controller can satisfy the stability and performance objectives.

- Chapter 4 summarizes the main contributions and achievements of this research. Furthermore, future research directions are outlined.

Chapter 2

Feasibility Analysis and Modeling

In this chapter, we present a feasibility analysis of application of solenoid actuators in transmission system of EVs. We determine the technical specifications required for the gear shifting task in an EV equipped with AMT and then we show that certain solenoid actuators are capable of meeting these technical requirements. Moreover, different modeling approaches are implemented and discussed.

2.1 Feasibility Analysis

Solenoid actuators provide several advantages in comparison to other types of actuators. This fact makes them an attractive option in the automotive industry. More specifically, due to the accessibility of electricity in EVs, the use of solenoid actuators for the gear shifting task in EVs seems reasonable. Therefore, we propose using solenoid actuators in EVs equipped with AMTs. The AMT studied here is located in the powertrain of an electric vehicle. Such AMT is made of a clutchless two-speed gearbox equipped with a solenoid actuator [38,39]. The feasibility of using this type of actuator in terms of providing required

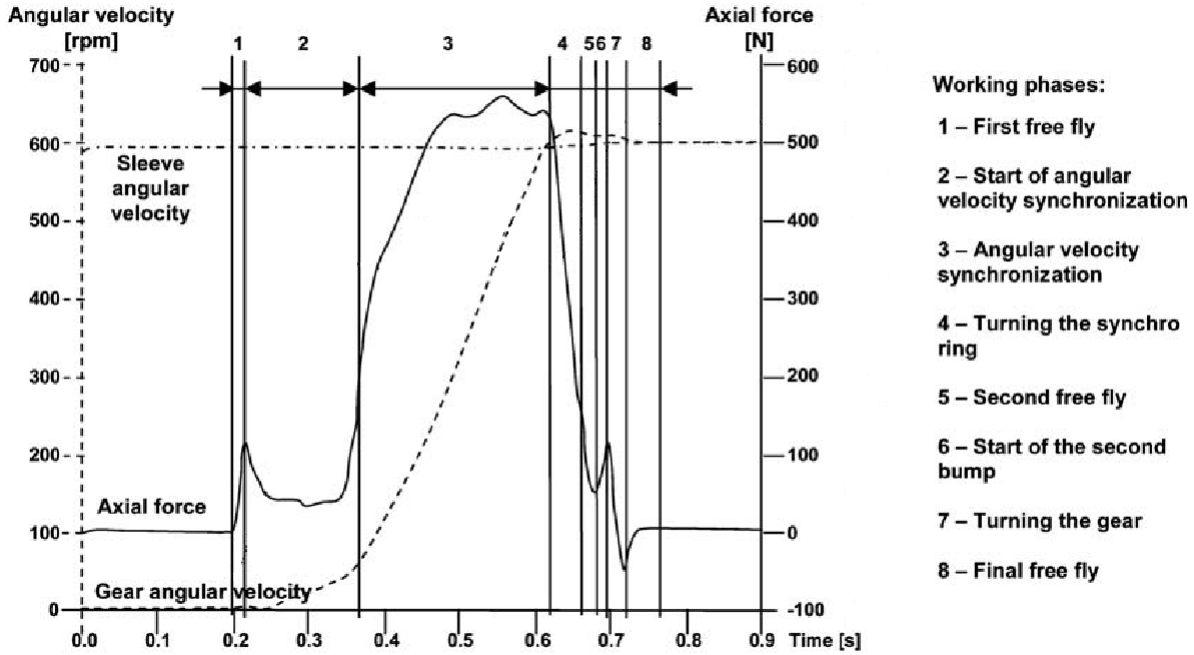

Figure 2.1 Axial force and angular velocity of the gear during gear shifting [40]

technical specifications for such application should be investigated. Hence, we need to know the required force profile for this task.

The principles of gear changing in AMTs are the same as in manual transmission systems. Therefore, the force requirements for gear shifting in AMTs is the same as in manual transmission system. In [40], the authors simulated the mechanical behavior of a synchronizer to improve the synchronization mechanism in a vehicle equipped with manual transmission. In this paper, the gear shifting cycle is divided into eight phases. The axial force and angular velocity of the gear have been measured and their variations during a gear shifting cycle are illustrated in Fig. 2.1.

In Fig. 2.1, it can be observed that the maximum required axial force that needs to be exerted on the synchronizer is around 500 N. This amount of axial force is used mainly in phase three of the gear shifting cycle. In this phase, the angular velocity of the synchronizer

sleeve and the gears are being synchronized. Also, it can be observed that the force should only be generated for a short period of time (less than 0.3 seconds). Hence, the actuator which is going to be selected to execute the gear shifting, should be capable of delivering high forces in a short period of time.

Furthermore, since the purpose of this thesis is to do the force control of the actuator used in the AMT system of an EV, we can assume that the plunger of the actuator is very close to where it wants to exert the force (*i.e.* synchronizer). From that point the actuator's force is going to be controlled. Hence, there is no limitation with regards to the stroke of the actuator.

Low profile [1] solenoid actuators provide high forces. Furthermore, they provide linear actuation and are very compact. Therefore, they will save some space for other components in the transmission system. The plunger of low profile actuators are built in both flat face and conical face. In Fig. 2.2, the two types of plungers in energized and de-energized states are illustrated. Conical face plungers provide longer strokes. However, when the actuator with this type of plunger is operated in small air gaps, it is more probable that the actuator will enter the saturation area comparing to the actuators with the flat face plunger. Saturation of magnetic material can reduce the efficiency of the actuator. Since the flat face plungers do not enter the saturation area very easily and we do not necessary need long strokes for our purpose, a low profile actuator with flat face plunger is chosen.

To choose the appropriate actuator among the low profile actuators with flat face plungers, it is very important to be aware of the performance requirements and operational limitations which are listed as follows:

- The required generated force is 500 N.
- The actuator should respond very fast to the force generation command.

1. low profile refers to a device that is wide in relation to its height

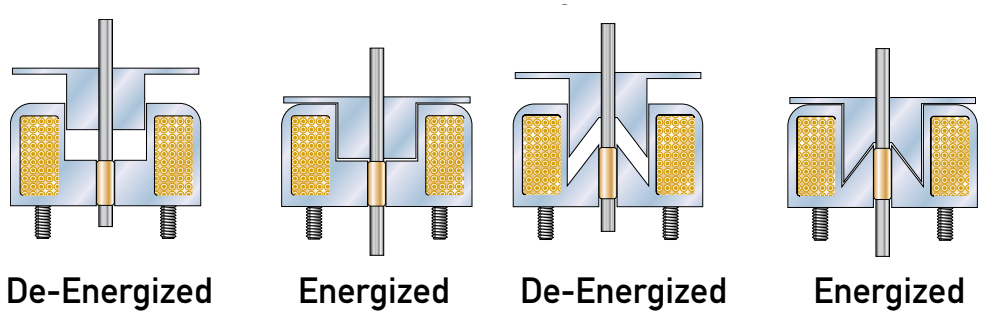

Figure 2.2 Solenoid actuator with flat and conical face plungers - Energized and De-energized states [41]

- The maximum time of the gear shifting is less than 1 second (see Fig. 2.1). Then the actuator should be able to keep generating the force for this time duration.
- The maximum voltage that the available power supply can provide is 33 V.

We select our solenoid actuator from the products of Ledex® company, which is a pioneer manufacturer in producing solenoid actuators for various applications. The solenoid actuator that meets the performance requirements and power supply limitations and is available for purchase is of class 6SFM. The performance specifications of this class of low profile actuators are presented in Table (2.1). The maximum voltage allowed to be applied for different coil turns and duty cycles are presented in Table 2.2.

For selecting the appropriate actuator for our purpose, the two tables should be regarded at the same time. For example, actuator awg #23 which has 432 turns operating with a PWM duty cycle of 50% can tolerate a maximum DC voltage of 14.6 V for 87 seconds (see Table 2.1). On the other hand, when this actuator is operating with a PWM duty cycle of 100%, the supplied voltage should not exceed 10.3 V; so it can be under operation infinitely. It can also be seen that the solenoid coil resistance is 3.59 Ω if the working temperature is 20°C.

The solenoid actuator force versus stroke graph for various duty cycles is illustrated in

Table 2.1 Solenoid Actuator Performance [41]

Maximum Duty Cycle	100%	50%	25%	10%
Maximum On Time (sec) when pulsed continuously	∞	87	36	13
Maximum On Time (sec) for single pulse	∞	140	44	16
Watts (at 20° C)	32	64	128	320

Table 2.2 Maximum allowed voltage for the actuator with different coil data [41]

awg #	Resistance (20°C)	Turns #	V_{DC} 100%	V_{DC} 50%	V_{DC} 25%	V_{DC} 10%
23	3.59	432	10.3	14.6	21.0	33.0
24	5.24	500	13.0	18.4	26.0	41.0
25	9.51	708	16.7	24.0	33.0	53.0
26	14.44	858	21.0	30.0	42.0	66.0
27	23.69	1110	27.0	38.0	53.0	84.0
28	38.27	14.11	34.0	48.0	68.0	106.0
29	54.62	1638	41.0	59.0	83.0	131.0
30	93.67	2184	53.0	76.0	107.0	168.0
31	143.00	2645	67.0	95.0	134.0	211.0
32	223.00	3328	83.0	118.0	167.0	262.0
33	338.00	4004	105.0	149.0	210.0	331.0

Fig. 2.3. It can be seen that the actuator generates higher forces when it is driven in lower duty cycles. The reason is that in the lower duty cycles higher voltages can be applied to the actuator. Therefore, stronger magnetic fields are generated and that will, in turn, produce higher forces. This figure also shows that if an actuator is operated in smaller strokes, it will produces higher forces comparing to when the stroke is longer.

Considering the performance requirements and limitations expressed earlier, the solenoid

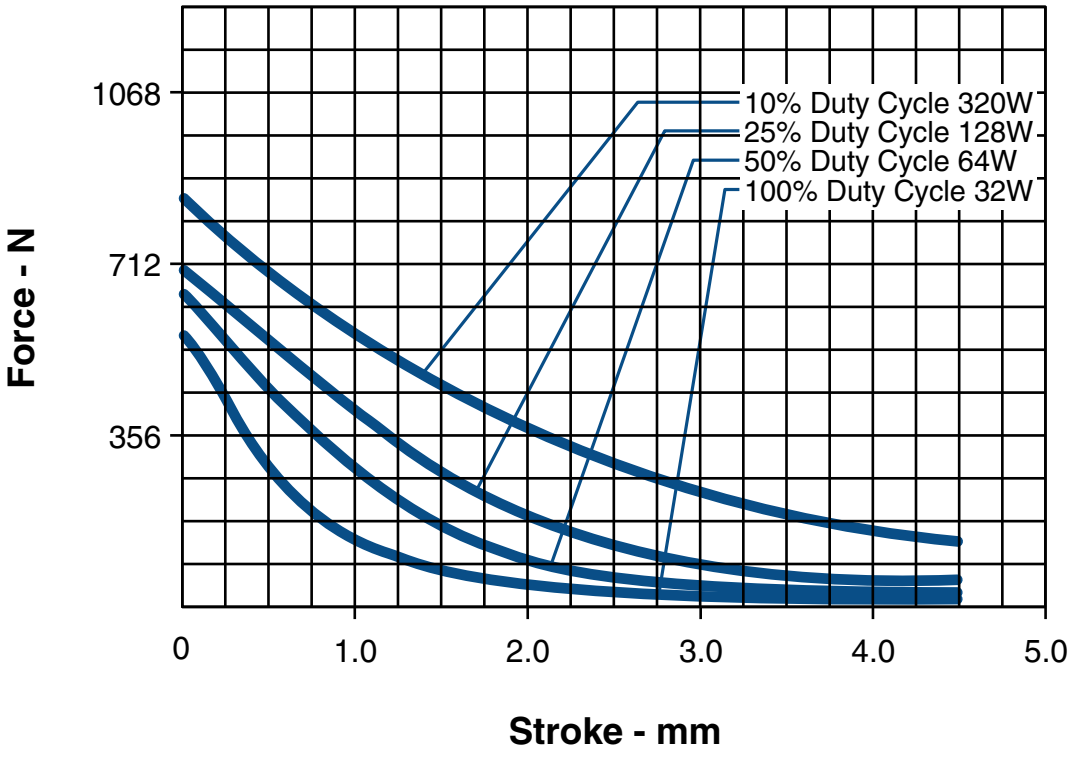

Figure 2.3 Solenoid actuator force versus stroke for various duty cycles [41]

actuator with awg #23 is selected. It will be operated in 10% duty cycle, and is supplied by DC voltage of up to 33 V that matches the available power supply. In these operation conditions, it will be able to produce the required 500 N force for the gear shifting purpose.

2.2 Modeling

The schematic of a solenoid actuator and its parts are shown in Fig. 2.4. As shown in this figure, a solenoid actuator consists of a coil which is a stationary part and is labeled number (7) in this figure. The coil is wound around a cylindrical metal rod. This rod or "plunger" is made of ferromagnetic materials. The plunger can enter or exit the coil without being in contact with it. In Fig. 2.4, this component is indicated by number (1). Other

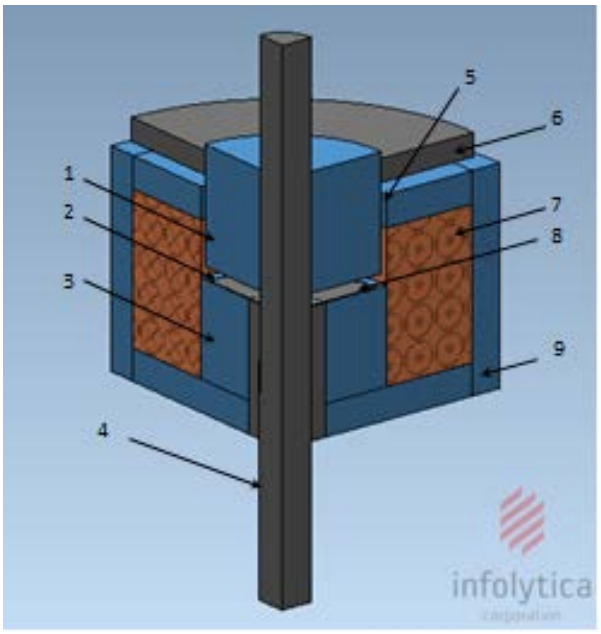

Figure 2.4 Solenoid Actuator Components

components of the actuator are main air gap (2), core (3), shaft (4), secondary air gap (5), cap (6), air gap spacer (8), and housing (9) and are shown in this figure. Applying an electrical current to a solenoid coil generates a magnetic flux whose intensity is proportional to the current. Such magnetic field pulls the plunger to intensify the field concentration inside the solenoid. Therefore, the EM force is created.

The purpose of this section is to propose a reduced-order model of the actuator. In order to drive a model which can accurately describe the actuator's behavior, several modeling approaches are used.

First, very general equations for simplifying the electric and magnetic interactions in an electromagnetic actuator are presented. However, these equations are useful to acquire a broad knowledge of electromagnetic properties in the actuator such as the relationships between force, voltage, current, and magnetic field, they may not represent the electromagnetic behavior of the actuator working in different situations. Since some assumptions are

made to derive these equations, such equations cannot be applied to all actuator operation conditions, *e.g.* saturation condition.

When the basic equations for describing the electromagnetic behavior of the actuator are presented, FEM modeling of the actuator is introduced as a reliable tool to model the electromagnetic behavior of the actuator. Basically, the electromagnetic behavior of any electromagnetic device is described by Maxwell's equations. Maxwell's equations consist of a set of complicated equations. These equations represent how the electric and magnetic fields interact. To find out the electromagnetic behavior of the actuator, the Maxwell's equations should be solved. Considering the tedious nature of solving these equations, FEM analysis is proposed for carrying out the calculations.

On the other hand, the model that the FEM approach suggests is not perfect for some conditions that may arise during the steady state operation of the actuator. For example, the variation of parameters in the steady state operation of the actuator is not modeled within FEM. To assure that the achieved model, which is going to be used for control purposes, is taking care of all the uncertainties in the systems, experimental results are used to identify accurate models representing solenoid actuator response in all possible operating conditions. In this thesis, this approach is called *experimental modeling approach*.

2.2.1 Simplified Theoretical Approach

Every ferromagnetic material has its own magnetization curve (B-H curve). In the B-H curve of a specific ferromagnetic material, increasing H up to a certain point (around the knee of the curve), results in increasing B linearly (linear region). Above the knee point on the curve, B cannot increase linearly with increases in the H anymore. In this region, the material is magnetically saturated (saturation region), *e.g.* Fig. 2.8 [42].

In this section, a generic model for calculation of the force and current of the actuator

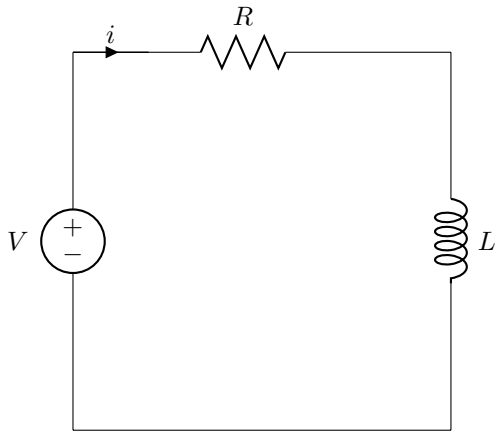

Figure 2.5 Electric equivalent circuit

is presented. In order to be able to develop this model, it is assumed that the actuator is working in the linear region, otherwise such model would not be obtained. Developing the electric circuit and equivalent electrical circuit of the magnetic system helps in understanding the interactions between the electric and magnetic fields.

Since we assumed that the actuator is working in the linear region, an inductance can be defined for the actuator. From the electrical circuit point of view, the equivalent circuit of the actuator can be seen at Fig.2.5.

The equivalent circuit is an $R-L$ circuit. A KVL in this circuit will result in:

$$V = Ri + L\frac{di}{dt} + i\frac{dL}{dt} \tag{2.1}$$

where L, R, i, and V are the solenoid coil inductance, solenoid coil resistance, current and input voltage, respectively. As L is a function of the air gap length x (This will be shown in developing the equivalent electrical circuit of the magnetic system and consequently where

the inductance formula (2.18) is derived), (2.1) can be rewritten in the form

$$V = Ri + L\frac{di}{dt} + i\frac{\partial L}{\partial x}\frac{\partial x}{\partial t} \tag{2.2}$$

Since in this study we are interested in modeling the actuator for force control applications, we assume that the actuator's plunger is not expected to move. In other words, we assume that the plunger has already moved to the desired position and the plunger is supposed to exert the force. Therefore, the $\frac{\partial x}{\partial t}$ term is negligible. (2.1) can be rewritten as follows

$$V = Ri + L\frac{di}{dt} \tag{2.3}$$

In the Laplace domain, the voltage-current relationship can be written as:

$$\frac{I}{V} = \frac{1}{R + Ls} \tag{2.4}$$

In order to develop the electrical equivalent circuit of the magnetic circuit of the actuator, two main assumptions are made.

- The actuator is working in the linear region, and
- There is no flux leakage.

To develop the circuit, we should know how the magnetic flux chooses its path in the actuator. Basically, the magnetic flux tends to follow the path with the least magnetic reluctance. Components made of ferromagnetic materials express much lower reluctances for the magnetic flux in comparison to the non-ferromagnetic materials. Hence, the magnetic flux tends to cross through ferromagnetic materials to strengthen the electromagnetic field.

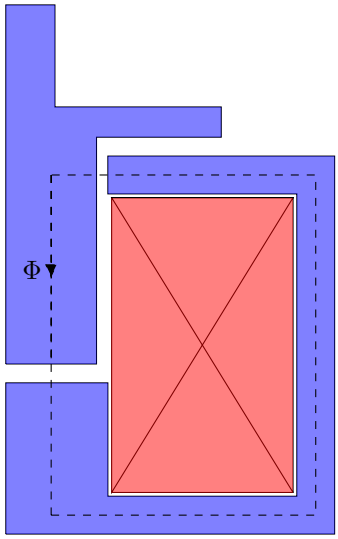

Figure 2.6 Magnetic circuit

A schematic of the half of the actuator's cross section is shown in Fig. 2.6.

The dashed line is the magnetic flux, crossing through the plunger and the housing. On its path, it has to cross two air gaps, namely, the main air gap, and the secondary air gap. We will see that the reluctances of these two air gaps play the most significant role in the amount of the generated flux.

From Fig. 2.6, we can see that the generated magnetic flux passes through four reluctances. Therefore, the electrical equivalent circuit can be derived as shown in Fig. 2.7.

In this figure, $\mathcal{F}$ is the magneto-motive force (MMF). $\mathcal{R}_c$ is the reluctance of the housing, $\mathcal{R}_x$ and $\mathcal{R}_g$ are the reluctances of the main air gap and the secondary air gap, respectively, and $\mathcal{R}_p$ is the reluctance of the plunger. Φ is the generated magnetic flux in Weber.

Magneto-motive force (MMF) is the equivalent of electro-motive force (EMF) in electric circuits. This MMF is the cause of magnetic flux generation. MMF is defined as:

$$\mathcal{F} = Ni \tag{2.5}$$

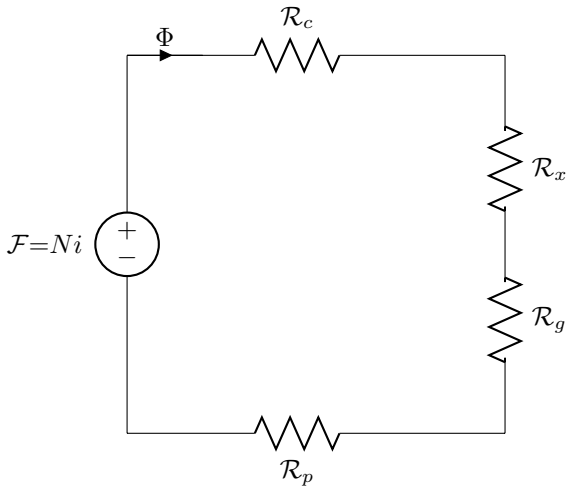

Figure 2.7 Equivalent electrical circuit

where N is the number of turns of the winding and i is the current going through the winding. The unit for $\mathcal{F}$ is Ampere-turns (At). Given the MMF of a magnetic circuit, the generated flux can be calculated using the following equation

$$\mathcal{F} = \mathcal{R}\Phi \tag{2.6}$$

where $\mathcal{R}$ is the total reluctance.

When 2.5 and 2.6 are combined with the definition of inductance,

$$L(x) = \frac{N\Phi}{i} \tag{2.7}$$

then, the inductance of the actuator can be calculated using the following equation

$$L(x) = \frac{N^2}{\mathcal{R}} \tag{2.8}$$

$\mathcal{R}$ can be regarded as the summation of reluctances of different components

$$\mathcal{R} = \mathcal{R}_c + \mathcal{R}_x + \mathcal{R}_g + \mathcal{R}_p \tag{2.9}$$

where $\mathcal{R}_c$ is the core reluctance, $\mathcal{R}_x$ is the reluctance of the main air gap, $\mathcal{R}_g$ is the reluctance of the secondary air gap and $\mathcal{R}_p$ is the reluctance of the plunger. The reluctances can be calculated as follows

$$\mathcal{R}_c = \frac{l_c}{\mu_f \mu_0 A_f} \tag{2.10}$$

$$\mathcal{R}_x = \frac{x}{\mu_0 A_f} \tag{2.11}$$

$$\mathcal{R}_g = \frac{g}{\mu_0 A_g} \tag{2.12}$$

$$\mathcal{R}_p = \frac{l_p - x}{\mu_f \mu_0 A_f} \tag{2.13}$$

where l_c is the effective length of the housing that the flux is going through. μ_f is the relative permeability of the electromagnetic material used in the actuator. μ_0 is the permeability of the free space. A_f is the cross sectional area of the plunger which is perpendicular to the flux path. x and g are the main air gap and the secondary air gap lengths, respectively. A_g is the effective area of the secondary air gap where the the flux is crossing. l_p is the effective length of the plunger when the main air gap x is zero.

Having 2.8 and 2.9, the reluctance of the actuator is calculated as

$$L(x) = \frac{N^2}{\mathcal{R}_c + \mathcal{R}_x + \mathcal{R}_g + \mathcal{R}_p} \tag{2.14}$$

The main air gap and the plunger reluctances are both dependent on the main air gap length. Therefore, the total inductance of the system is a function of the length of the

main air gap. Hence, as the plunger moves forward or backward, the main air gap length changes and consequently the actuator's inductance varies. We assumed that the actuator is working in the linear region, therefore we have

$$B = \mu_f \mu_0 H \tag{2.15}$$

where B and H are the flux density and the magnetic intensity, respectively. Also, for the electromagnetic materials we have

$$\mu_f >> 1. \tag{2.16}$$

Therefore, R_c and R_p are negligible comparing to R_x and R_g and can be ignored. (2.14) can be rewritten as

$$L(x) = \frac{N^2}{R_x + R_g} \tag{2.17}$$

Substituting (2.11) and (2.12) in (2.8), we will have

$$L(x) = \frac{N^2 \mu_0 A_f A_g}{A_f g + A_g x} \tag{2.18}$$

On the other hand, the electromagnetic force can be calculated as follows [43]

$$F_e = \frac{\partial W_c(i,x)}{\partial x} \tag{2.19}$$

where W_c is co-energy which is used to calculate the electromagnetic force produced by the actuator. Co-energy is a concept which is useful in calculating mechanical forces in

electromagnetic devices. Assuming there is no energy loss, the input energy would be stored as electromagnetic energy in the core. Then, based on the co-energy definition, the stored energy is equal to the co-energy.

Since it is assumed that the actuator is operated in linear region and no energy is wasted, the co-energy formula can be written as

$$W_c(i,x) = \frac{1}{2}L(x)i^2 \tag{2.20}$$

Then, substituting (2.20) in (2.19), the electromagnetic force can be calculated as

$$F_e(i,x) = \frac{1}{2}i^2\frac{\partial L}{\partial x} \tag{2.21}$$

Substituting L from 2.18 in 2.21 the electromagnetic force formula will be

$$F_e(i,x) = -\frac{1}{2}i^2\frac{N^2\mu_0 A_f A_g^2}{(A_f g + A_g x)^2} \tag{2.22}$$

In calculating the electromagnetic force, some parameters, such as g, play a significant role in the amount of the electromagnetic force produced. So, the accuracy of force calculations depend on how accurate those parameters are measured. To ensure that the calculations are accurate, (2.23) can be used

$$F_e = -\frac{1}{2}i^2\frac{\gamma}{(\alpha + \beta x)^2} \tag{2.23}$$

where α, β, and γ are functions of the number of coil turns, magnetic materials properties, and geometry of the actuator components. By substituting three sets of current, air gap, and force measurements, α, β and γ can be calculated. Therefore, (2.23) expresses the

electromagnetic force relationship with the air gap length and current.

As mentioned earlier, this approach is developed under limited actuator operating conditions, which makes the model not to be useful for all operating conditions. In other words, the operation of the actuator in the linear region is not guaranteed, *i.e.*, there is a possibility that the actuator operates in the saturation region, which means that (2.3) and (2.23) are not valid any more. Moreover, there is always some flux leakage, which in this approach are ignored. This will affect the accuracy of the developed model. To develop a reliable model for the actuator, alternative approaches are chosen. The two approaches used here to determine the electromagnetic behavior of the solenoid actuator are the following

- Finite Element Method (FEM), and
- Experimental approach.

2.2.2 Finite Element Method Approach

FEM is a tool for solving a wide range of research and industry problems including electric and magnetic fields problems. It is a numerical technique which finds the approximate solution to the boundary condition problems for partial differential equations [44]. In this technique, the field equations of a problem are discretized using piecewise polynomial interpolation.

To investigate the electromagnetic behavior of an electromagnetic device, Maxwell's equations should be solved. FEM enables the user to solve these equations using several optimization methods. This includes solving simultaneous partial differential equations, under predefined boundary conditions. In this thesis, the finite element analysis is conducted using the FEM software developed by Infolytica called MagNet® [45]. The general 3D analysis is based on the $T - \Omega$ method [46, 47]. In this method, the field intensity

vector, $\boldsymbol{H}$ and the electric conductors current density vector, $\mathbf{J_e}$ are expressed in terms of the unknown total scalar potential, Ω, (2.24), and the current vector potential, $\boldsymbol{T}$, (2.25), respectively.

$$\mathbf{H} = -\nabla\Omega \tag{2.24}$$

$$\mathbf{J_e} = \nabla \times \mathbf{T} \tag{2.25}$$

Basically, the fundamental principle in this technique is to divide the whole model into a mesh of elements and iteratively solve the Maxwell's equations for each node of the corresponding element. The flux density is calculated by solving the following equation

$$\nabla \times (\sigma^{-1} \cdot \nabla \times \mathbf{H}) + \mu \frac{\partial \mathbf{H}}{\partial t} = 0 \tag{2.26}$$

where σ is the electrical conductivity and μ is the permeability at each node.

The type of materials used in each component of the actuator are known. Also, the geometry of the actuator is measurable. Therefore, enough information is available to model the actuator in the FEM environment. Considering the cylindrical shape of the actuator, the accuracy of the FEM analysis is improved by modeling the system in three dimensions (3D). Since the actuator is an axisymmetric object, a quarter of the actuator is modeled along with the surrounding air. This reduces the required computation and the post-processing time. The specifications for the materials used in the components of the actuator are listed in Table 2.3.

Cold rolling, in Table 2.3, is referring to the process of rolling a material below its recrystallization temperature. This process increases the strength and hardness of the

Table 2.3 Solenoid Actuator Components Material

Component	Material
Plunger	12L14 Cold Rolled Steel
Core	12L14 Cold Rolled Steel
Housing	12L14 Cold Rolled Steel
Shaft	303 Stainless Steel
Cap	400 Series Stainless Steel
Air gap spacer	300 Series Stainless Steel

material and decreases its flexibility. Moreover cold rolling helps in producing the plate or sheets with the desired physical dimensions.

Cold rolled steel 12L14 is essentially a type of lead-added carbon steel which is re-sulfurized and re-phosphorized. The impact of adding lead along with the high levels of sulfur and phosphorous is to create a lubricating effect. This will result in a low friction, smooth and machined surface which would prolong its life time. Furthermore, this material is accounted as a ferromagnetic material which plays a significant role in intensifying the magnetic field. As mentioned earlier in Section 2.2.1, the components made of such a material provide the path with the least reluctance. Therefore, the flux goes mostly through the ferromagnetic components. The B-H curve of 12L14 Cold Rolled Steel is shown in Fig. 2.8.

Fig. 2.9 illustrates the geometry of the actuator. It can be seen that the actuator is indeed compact as we expect from a low profile flat faced actuator. In addition to occupying a small space, the compact design will reduce the gear shifting system weight, as well.

The MagNet® FEM solver uses the Newton-Raphson method to linearize the $B - H$ curve around the operating point and to iteratively update the permeability in the elements of the model. In this analysis, Newton tolerance, conjugate gradient tolerance, maximum

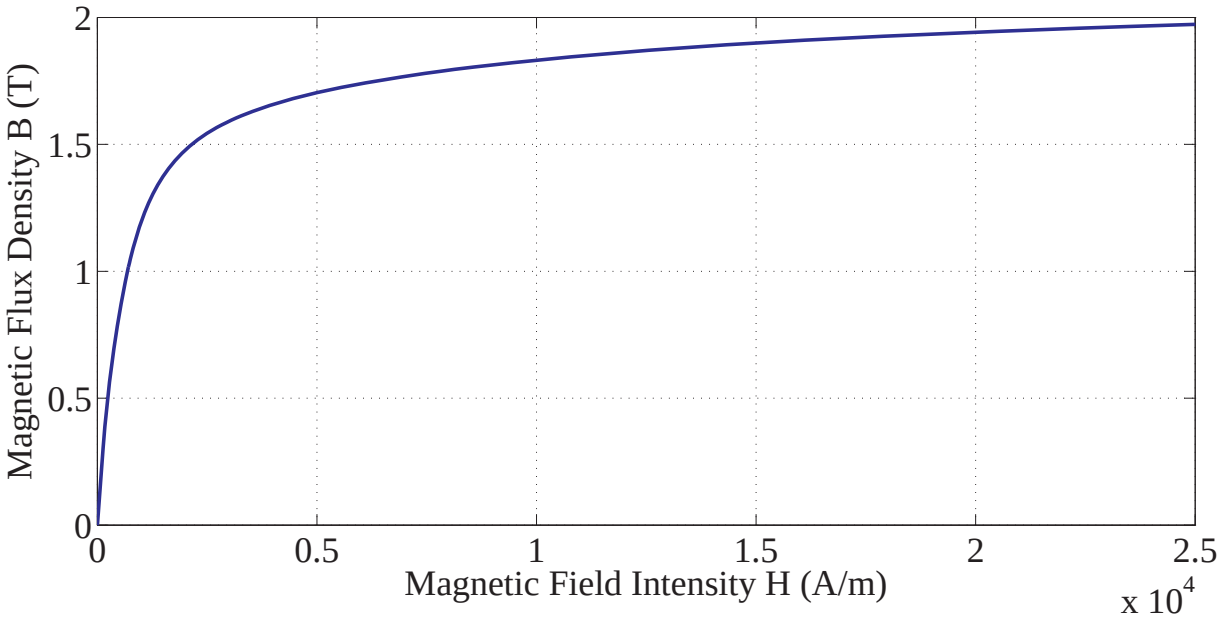

Figure 2.8 12L14 Cold Rolled Steel B-H curve

number of iterations, time step, and polynomial order are selected to be 1%, 0.01%, 20, 0.003 s, and 2, respectively.

In this analysis, the model is divided into a mesh of four-nodes tetrahedral elements. The accuracy of the solution depends upon two main factors: the nature of the field and the size of the mesh elements. In regions where the direction or the magnitude of the magnetic field is changing rapidly, high accuracy requires smaller elements. In order to create a mesh with high density in some areas, one should assign maximum element size to that area. There is always some trade-off between the accuracy and the computation time. As the meshing gets finer, the time spent for each iteration increases and this will significantly affect the solution time. We decreased the meshing size to the point that decreasing it more did not improve the accuracy of the results.

In this analysis, we assign a small maximum element size mostly to the magnetic components whose magnetic fields change significantly. Maximum element size of the coil and

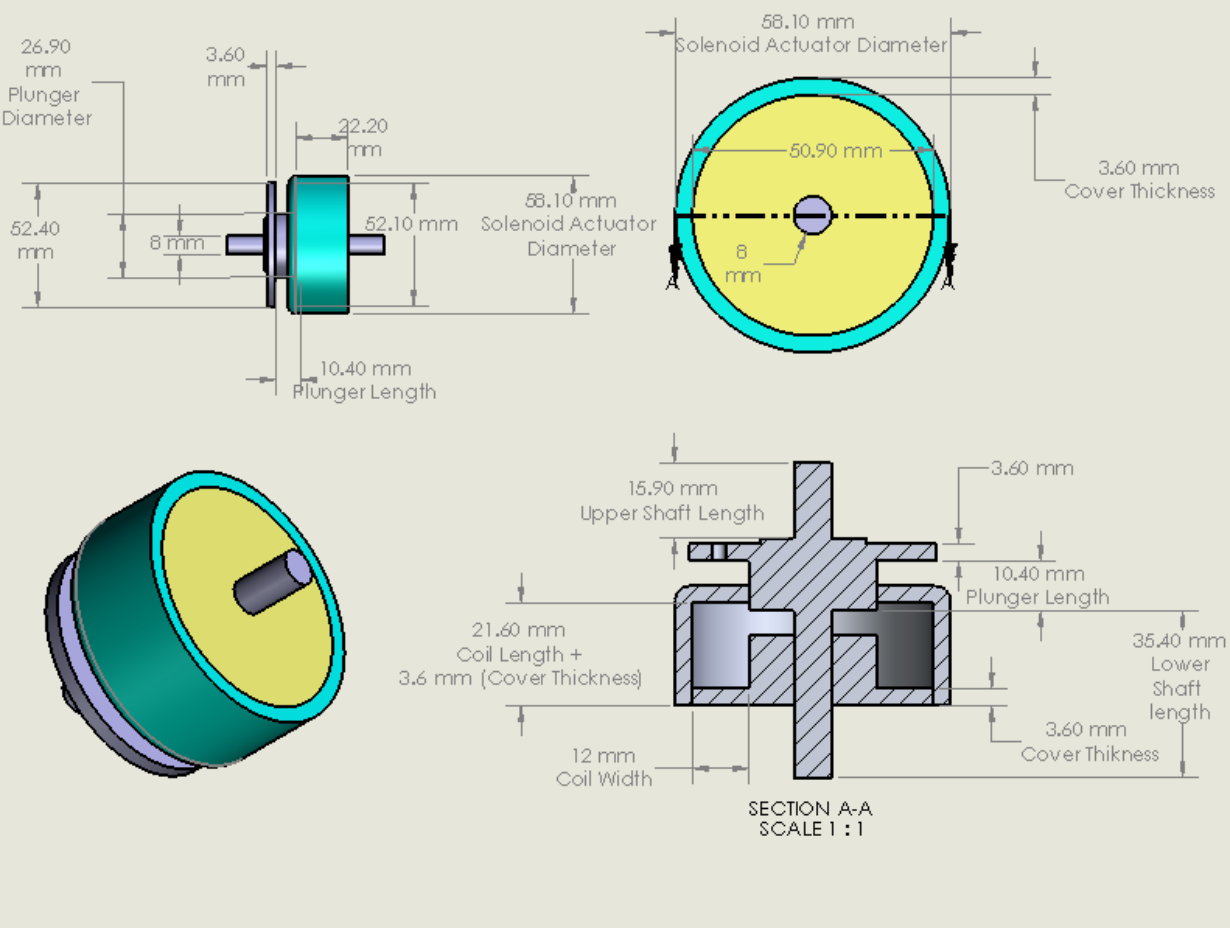

Figure 2.9 Solenoid actuator geometry

the air box is selected to be 5 mm, while the maximum element size of all other components is considered to be 1.75 mm. The mesh diagram of a quarter of the actuator is shown in Fig. 2.10.

As can be seen in Fig. 2.10, the meshing is finer at plunger, housing and core. Since these components are made of ferromagnetic material, the magnetic field density is higher in them. Therefore, we require finer meshing. On the other hand, it can be seen that meshing in the surrounding air box and the coil is coarser.

In terms of the supplied voltage, it is assumed that the actuator is supplied by 26.7 V

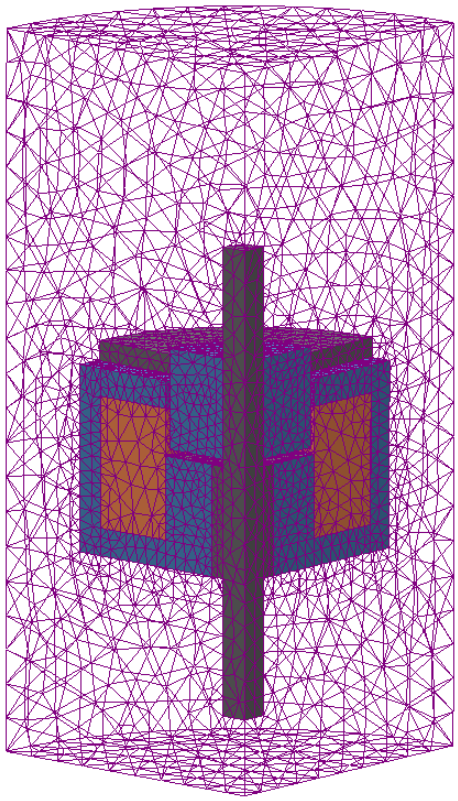

Figure 2.10 Mesh diagram of one quarter of the solenoid actuator

voltage. This is because the available driver can supply up to 26.7 V. As was mentioned earlier, by exploiting the axisymmetric feature of the actuator, only one quarter of the actuator is modeled in the FEM. Therefore, when doing simulations, the model is supplied by only one fourth of the total voltage, which is 6.675 V. The main air gap length is changed from 0.5 mm to 1.5 mm in 0.5 mm increments.

Fig. 2.11 shows the current provided by the power supply for different air gap lengths. This figure confirms that due to variations in the main air gap length, the current graphs are not identical in terms of the response time. The graph associated with longer lengths of the air gap have shorter response times. Despite the fact that the response time is sensitive to the air gap length variations, it can be seen that the steady state values of the current

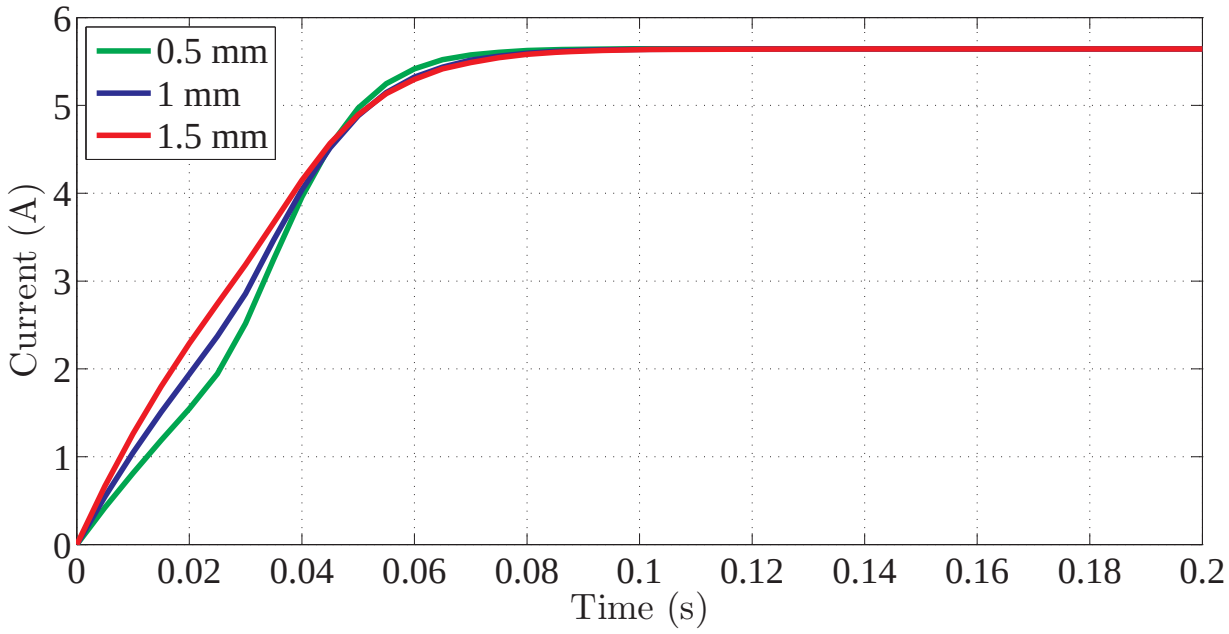

Figure 2.11 Current graphs for various main air gap lengths - FEM results

is the same. Since the resistance of the coil is the key factor in steady state value of the current and it was fixed under different operating conditions, then the steady state value of the current is not affected.

Fig. 2.12 shows the flux linkage in the actuator for different air gap lengths. It can be seen that as the air gap becomes shorter, the flux linkage, λ, increases. This means that as the air gap length decreases, the total reluctance of the actuator decreases and consequently, a stronger magnetic field is generated in the actuator. Since the flux linkage is proportional to the magnetic field density, decrease in the length of the air gap will result in higher flux linkages. Moreover, we can see from Fig. 2.12 that unlike the electric current, the steady state values of flux linkages are not the same.

Fig. 2.13 shows the electromagnetic force developed by the actuator for various air gap lengths. It can be seen from the figure that there is a direct relationship between the flux linkage and the electromagnetic force produced. Also, as mentioned earlier there is

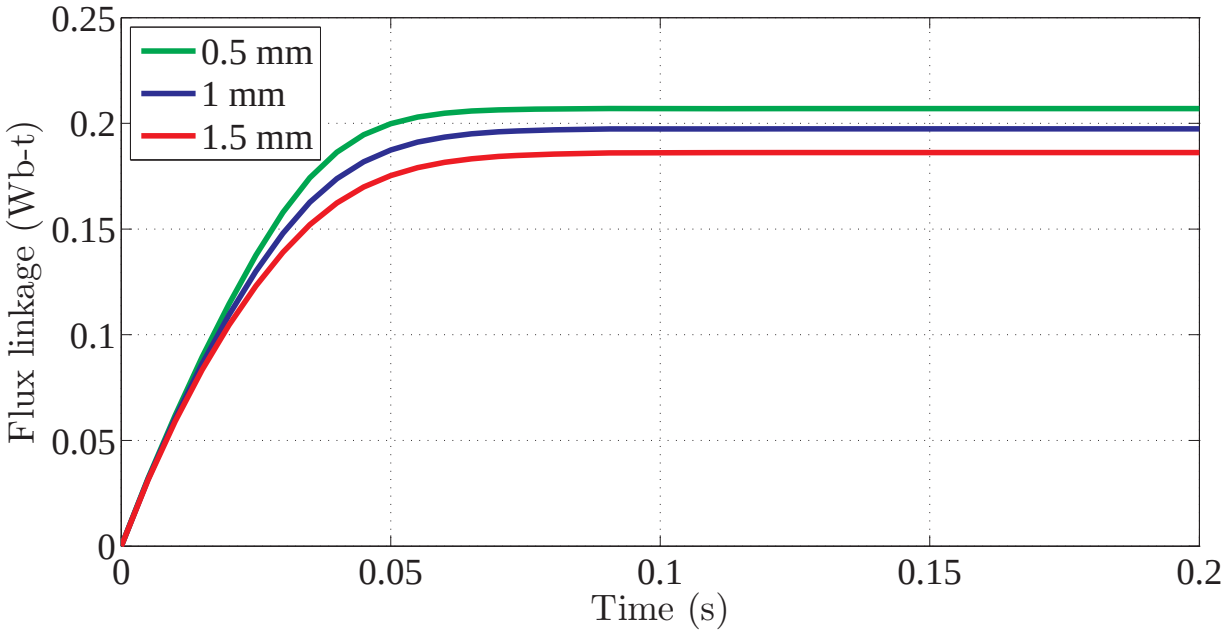

Figure 2.12 Flux linkage graphs for various main air gap lengths - FEM results

an inverse relationship between the main air gap length and the flux linkage. We can see from this figure that the same relationship holds for the developed force. In other words, as the air gap becomes smaller, the magnetic field becomes stronger and greater forces are produced in response to the high intensity of the magnetic field.

Fig. 2.14 shows the plot of the smoothed absolute values of the flux density ($|B|$) for various lengths of the main air gap. It can be seen that as the plunger moves closer to the core, *i.e.* as the air gap length decreases, the flux density increases. Also, we can see from the $B-H$ curve of the magnetic material, shown in Fig. 2.8, that when the magnetic flux density, $|B|$, increases to more than 1.5 T, the ferromagnetic material is operated in the saturation region. Looking at the color bar and smoothed $|B|$ shaded plot of Fig. 2.14 confirms that, for smaller main air gaps, the flux density of some regions of the actuator's ferromagnetic components are greater than 1.5 T (orange areas), and thus they are indeed

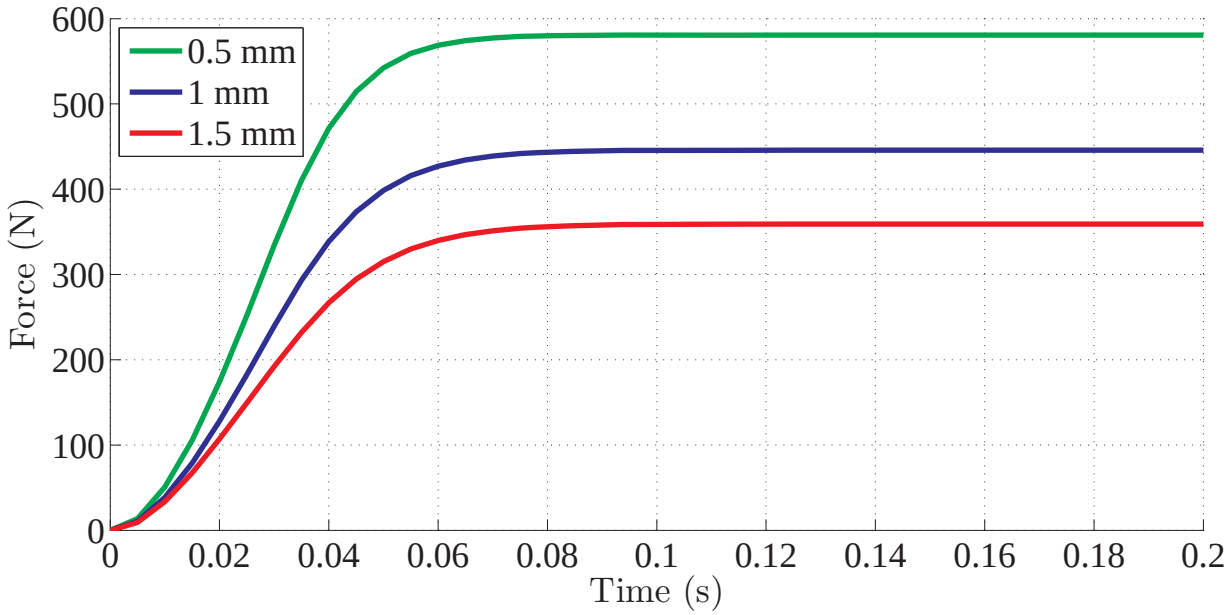

Figure 2.13 Developed force for various main air gap lengths - FEM results

working in the saturation region.

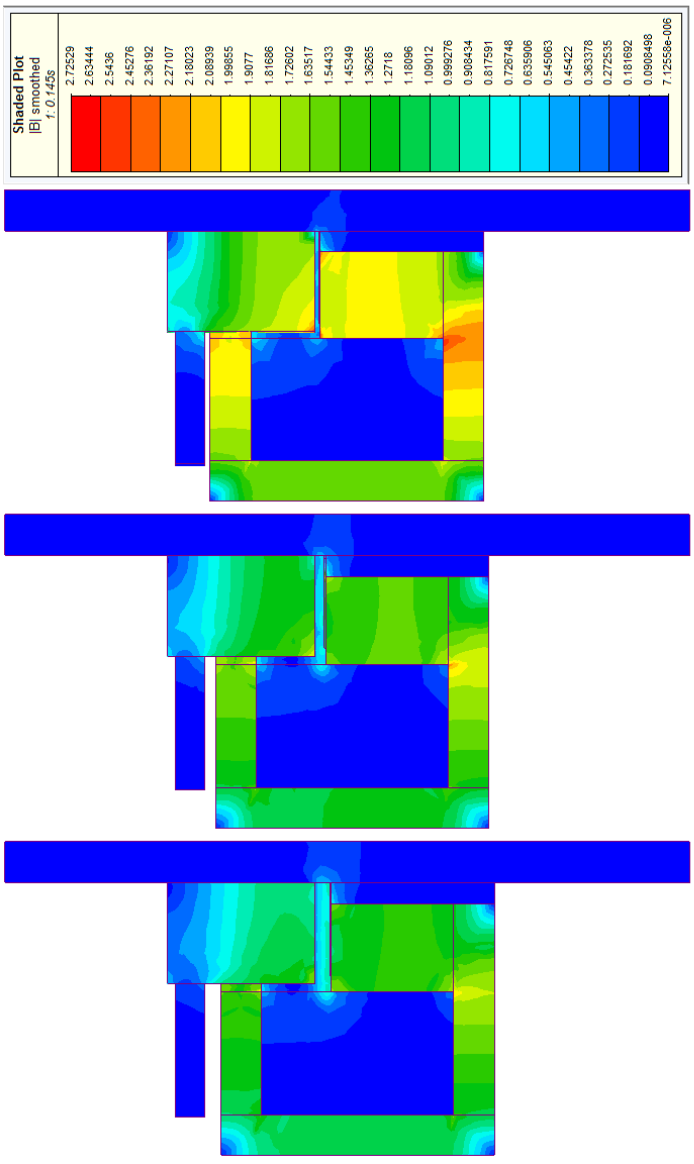

Figure 2.14 Shaded plot and contours of $|B|$ smoothed for main air gap lengths of (a) 1.5 mm, (b) 1 mm, and (c) 0.5 mm

In the theoretical approach proposed in Section 2.2.1, it was assumed that no saturation would happen. On the other hand, from the FEM analysis we can see that saturation is inevitable, especially when the actuator is working under high currents and short air gap lengths. These findings corroborate the decision to consider other approaches rather than a pure theoretical approach.

2.2.2.1 FEM Result System Identification

As discussed before, FEM is a reliable tool in comparison to the simplified theoretical approach. It is able to analyze the behavior of the solenoid actuator operating in saturation region. Although the numerical results of the FEM method are useful, they do not provide a suitable model for the purpose of controller design. Thus, based on the results of this method, system identification is performed in order to obtain an accurate model of the system.

Several approaches are available for the purpose of system identification, such as instrument variable, state variable filters, generalized Poisson moment functions and subspace state-space estimation. In this study, instrument variable approach [48] is used to estimate a transfer function. From the electrical behavior point of view, it was seen that the actuator's behavior resembles a simple first order system, *i.e.* one pole without any zero, see Fig. 2.11. Then, such a system is fitted to the results from the FEM analysis, when the air gap is 1 mm. The estimated first order system is as follows

$$\frac{I}{V} = \frac{7.629}{s + 35.31} \tag{2.27}$$

The magnitude bode diagram of the transfer function estimated from the current resulting from a step input of voltage is shown in Fig. 2.15. The blue region surrounding the

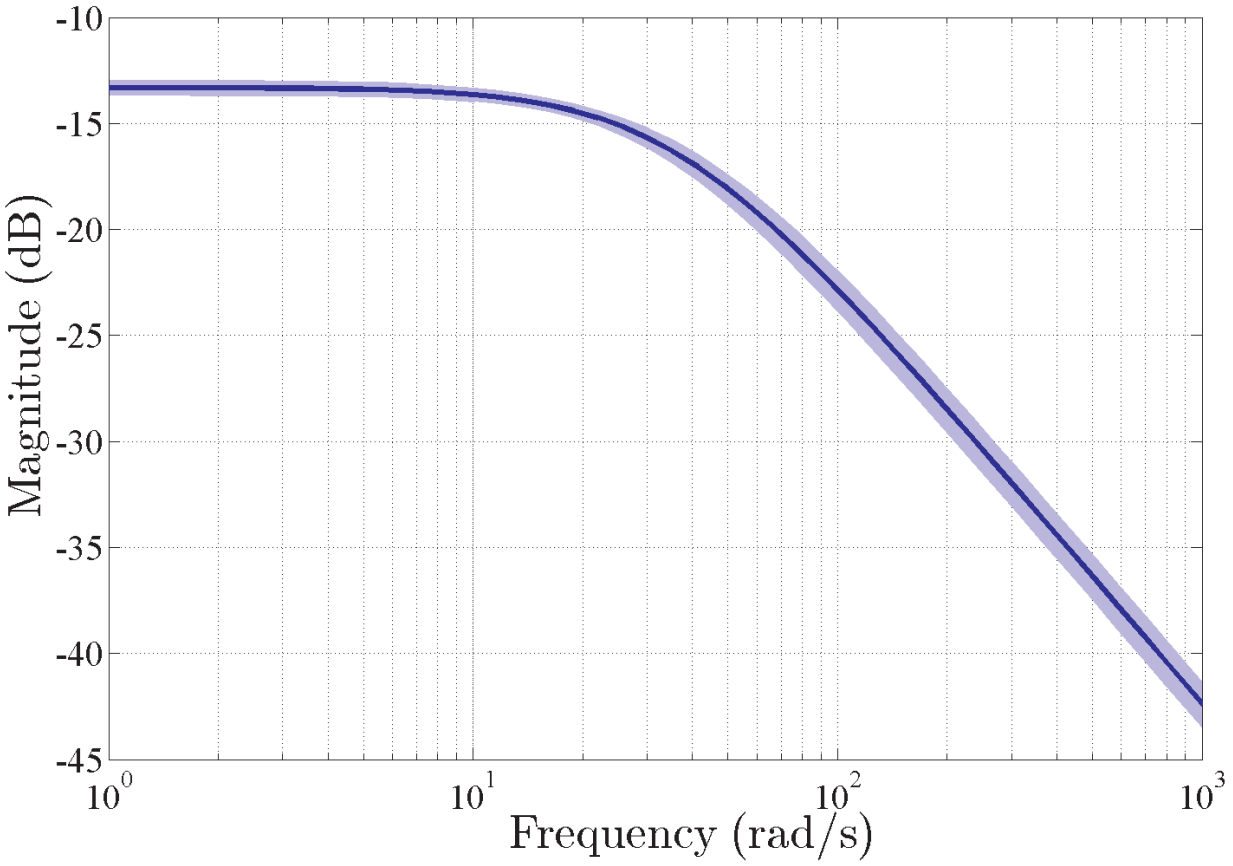

Figure 2.15 Magnitude bode plot of the estimated transfer function along with the confidence region

magnitude bode diagram of the system is the estimated region for the identified solution. This region is called *confidence region*. In this system identification process, the estimated transfer function is obtained after 2 iterations and is %85.57 fitted to the estimation data. Also, final prediction error (FPE) was 0.0615.

2.2.3 Experimental Approach

Despite the fact that FEM is a powerful tool in analyzing the electromagnetic behavior of the solenoid actuator, there are some downsides to this analysis method. For instance, there is always some measurement errors, especially in the actuator dimensions. Due to the

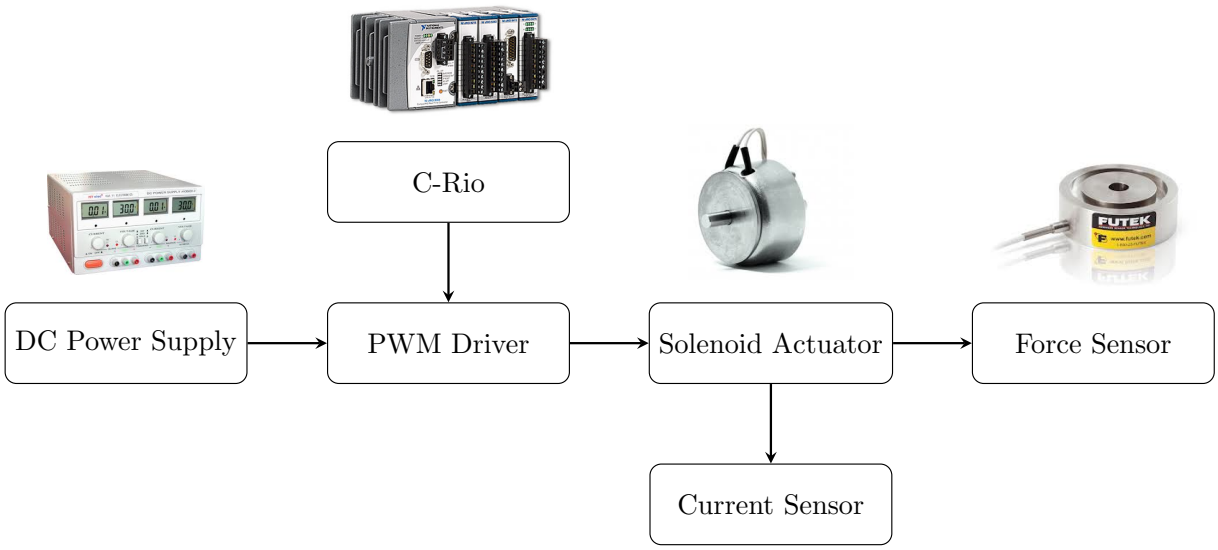

Figure 2.16 Experimental approach flow chart

sensitivity of the electromagnetic fields and consequently the sensitivity of the FEM results to the accurate measurement of dimensions of the components, the results from the FEM analysis could include some uncertainty. Also, there are some parameter variations such as temperature changes which could affect the operation of the solenoid actuator. Although FEM neglects the effects of the aforementioned uncertainty sources in the modeling of the actuator, the obtained results will still be used for controller design purpose.

Considering uncertainty sources involved in the modeling of the actuator, experimental approach is selected to compensate all the effects due to parameter uncertainties. Moreover, this approach will be used to verify the models from the preceding approaches. In this section, the experimental tests are conducted to investigate these variations and to achieve a reliable model for the solenoid actuator.

In order to perform the experimental tests, essential components such as power supply, real time computer, driver, and sensor are needed. The flowchart in Fig. 2.16 shows the interactions between the different components in the experimental testbed.

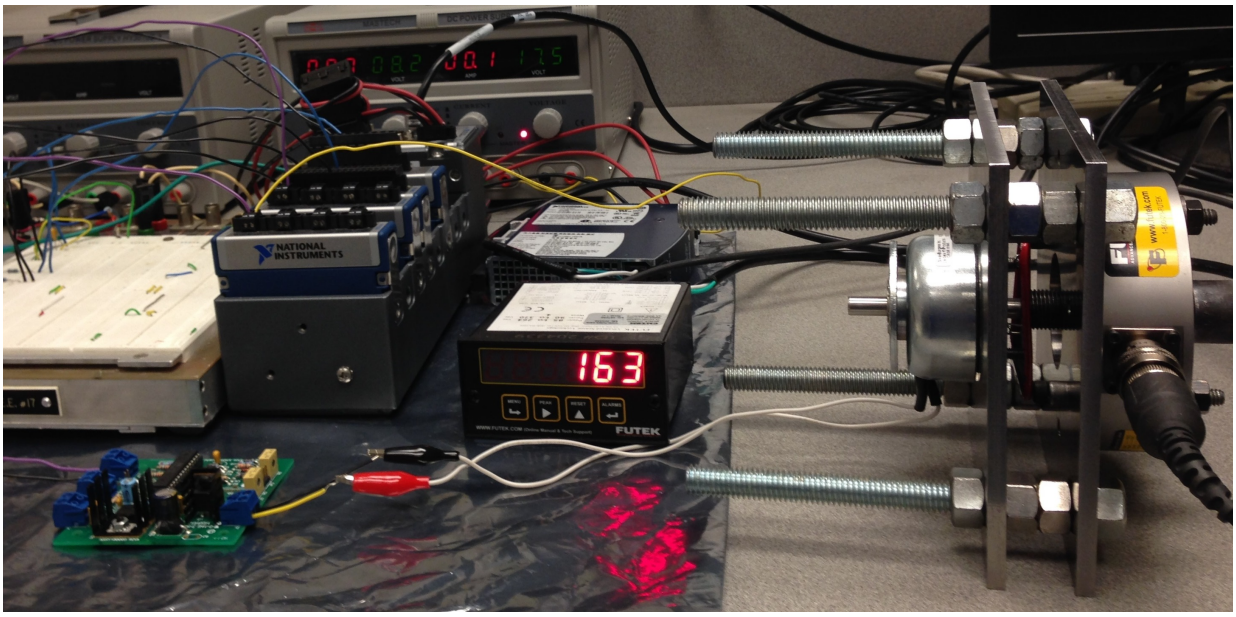

Figure 2.17 Experimental setup

The real time computer is a CompactRio® from National Instruments. The user determines what input voltage should be supplied to the actuator. The real time computer task is to receive the desired voltage from the user and to generate the equivalent DC command. The actuator is controlled via a Pulse Width Modulation (PWM) driver. The driver is supplied by the DC power supply and receives DC commands from the real time computer. Based on the command it receives, 25 kHz pulses with a specified duty cycle are produced. The actuator is supplied by the pulses from the driver and its force is measured using a force sensor with 1 N resolution. Fig. 2.17 shows the actual experimental setup.

As mentioned earlier, the main reason for developing this approach is that the FEM analysis is not able to consider the effects of the parameter changes. For example, coil resistance is influenced by variations in temperature that the actuator is operating at. The

resistance is a linear function of the temperature variation as shown in the following

$$R = R_0(1 + \alpha(T - T_0)) \tag{2.28}$$

where α is the temperature coefficient of the resistance, R_0 is the initial value of the coil resistance at temperature T_0, and R is the coil resistance at the new temperature T.

When the actuator is in operation, there are some losses which are the main reason for temperature increase in the actuator and consequently in the coil. The losses are composed of the copper loss, calculated by (2.29), and the iron loss which are decomposed into hysteresis and anomalous loss and eddy current loss and are calculated by (2.30).

$$P_{copper} = Ri^2 \tag{2.29}$$

$$P_{core} = K_h f^{\alpha} {B_{pk}}^{\beta} + K_e (sfB_{pk})^2 \tag{2.30}$$

where K_h and K_e are the hysteresis and eddy current coefficients, respectively. α is the frequency exponent, β is the flux density exponent, s is the lamination thickness ratio, and B_{pk} is the peak AC flux density. Since there is an interaction between the thermal and magnetic behavior of the actuator, the rise in the actuator's temperature would itself affect the electromagnetic behavior of the actuator. This interaction is not taken into account in the FEM approach.

To prove that the actuator's temperature is influenced when it is under operation, the current graph obtained in the experimental test is presented in Fig. 2.18.

In this graph, the air gap length is set to be 0.5 mm and the supplied voltage is 26.7 V. It can be seen that the actuator has been under operation around four seconds, and

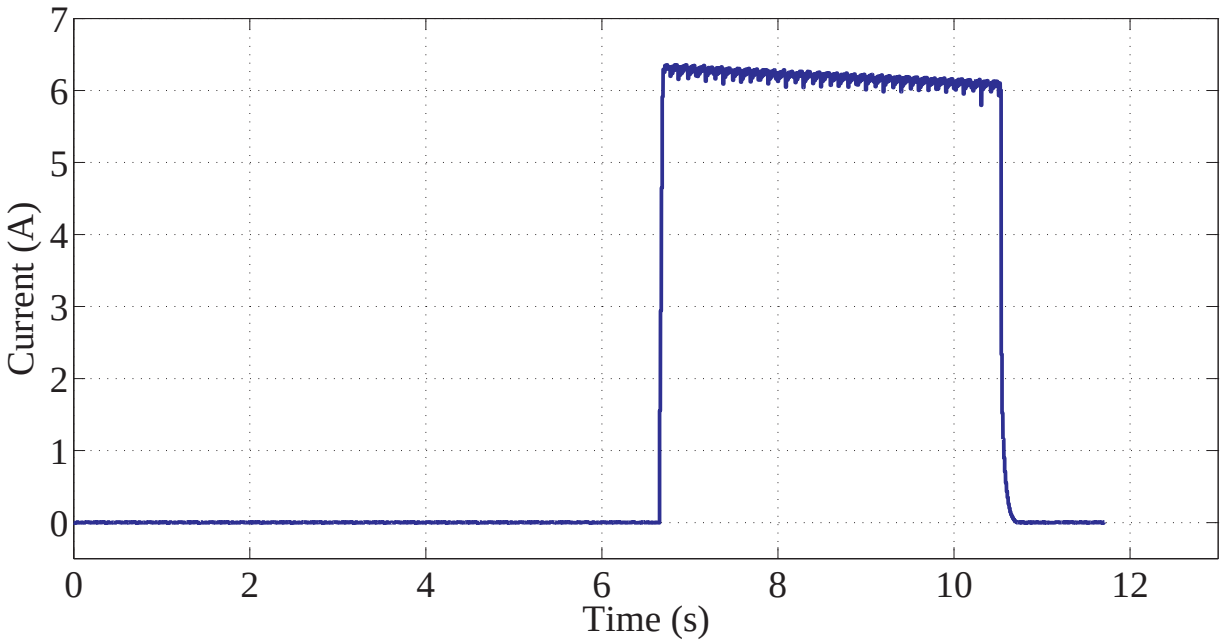

Figure 2.18 Temperature rise effects on the actuator current

the current is affected by the temperature rise in the actuator. During this short amount of time, the current is decreased by 10%. During the same period of time, we observed an average coil resistance increase of 12%. Given that the initial resistance of the coils before the experiment was 3.7 Ω and that the temperature coefficient of copper is 0.0039 K^{-1}, using (2.28), we can calculate that the temperature rise of the coils is about 31°C.

The experimental tests are performed for three main purposes,

1. Air gap spacer impact investigation
2. Dynamic modeling of the actuator
3. Static modeling of the actuator

2.2.3.1 Impact of Air Gap Spacer

As it can be seen in Fig. 2.4, there is an air gap spacer in the actuator which is mainly responsible for setting a gap between the ferromagnetic plunger and the ferromagnetic core. As can be seen in Table 2.3, the air gap spacer is made of 300 series stainless steel and is non-magnetic. Several experiments are performed to investigate if using this spacer would have impacts on the amount of electromagnetic force generated. The tests are carried out for the air gap lengths of 0.5 mm to 3.5 mm with increments of 1 mm. The supplied voltage has been set to be 10, 20, and 26.7 V. In each experiment, the current and force are measured with and without the air gap spacer. The current and force graphs are plotted for each air gap length. Figs. 2.19–2.22 show the source current for each air gap length. Similarly, Figs. 2.23–2.26 show the force measurements for each air gap length.

Examining the current graphs shows that the steady state values of the current is not

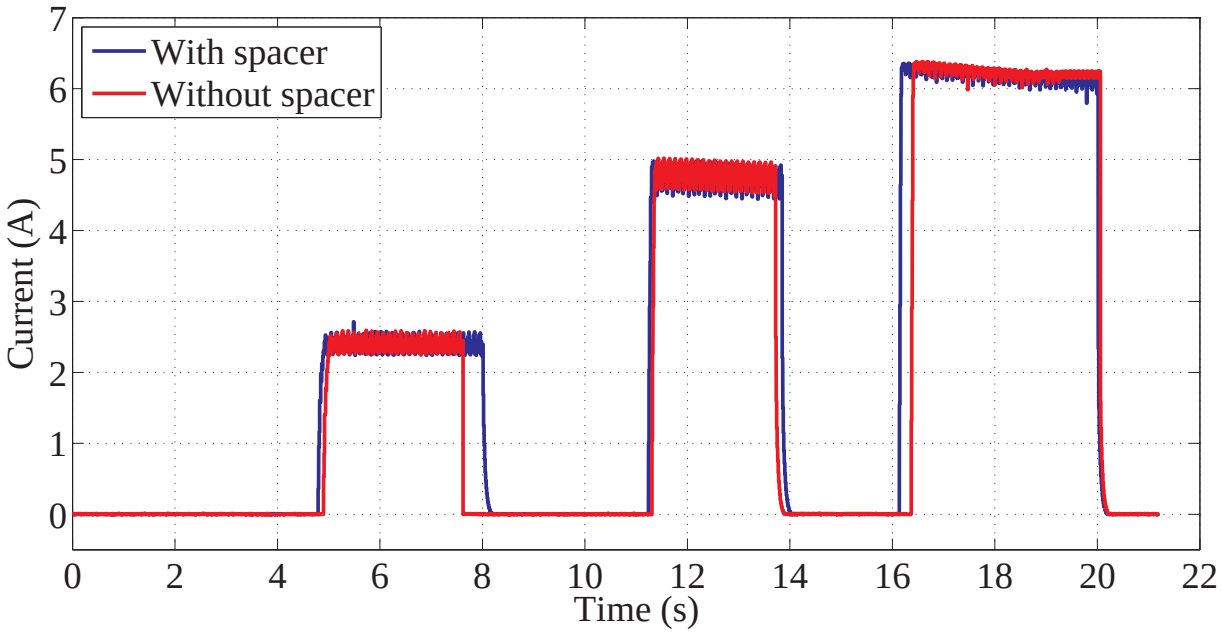

Figure 2.19 Measured current of the actuator with and without the air gap spacer - Air gap length 0.5 mm

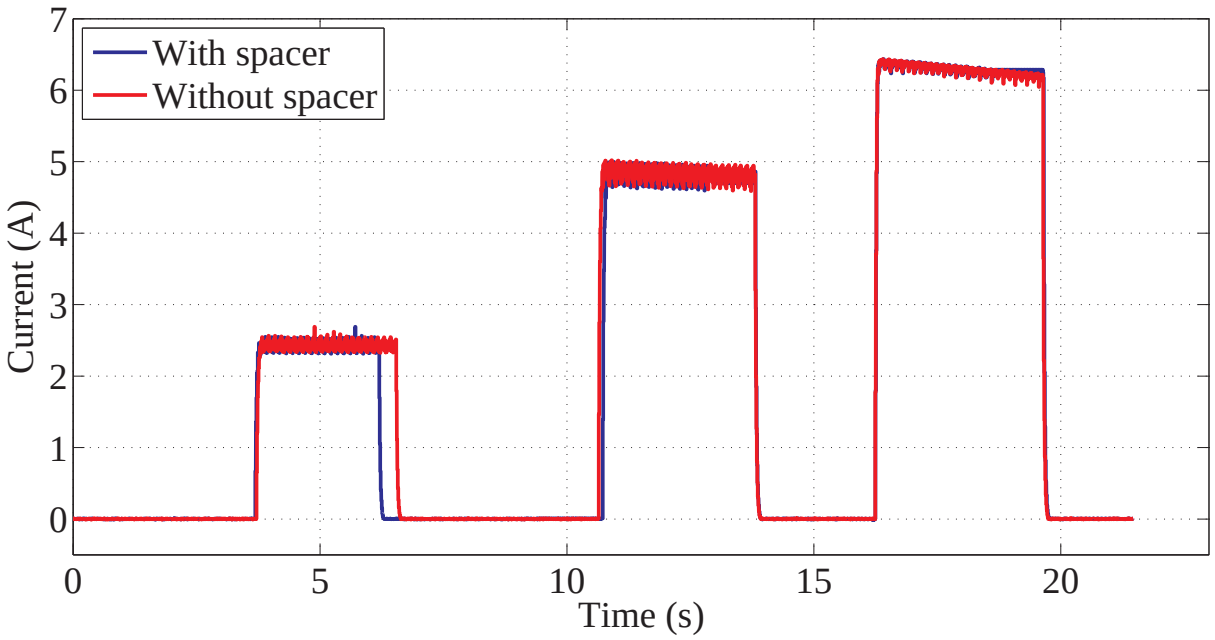

Figure 2.20 Measured current of the actuator with and without the air gap spacer - Air gap length 1.5 *mm*

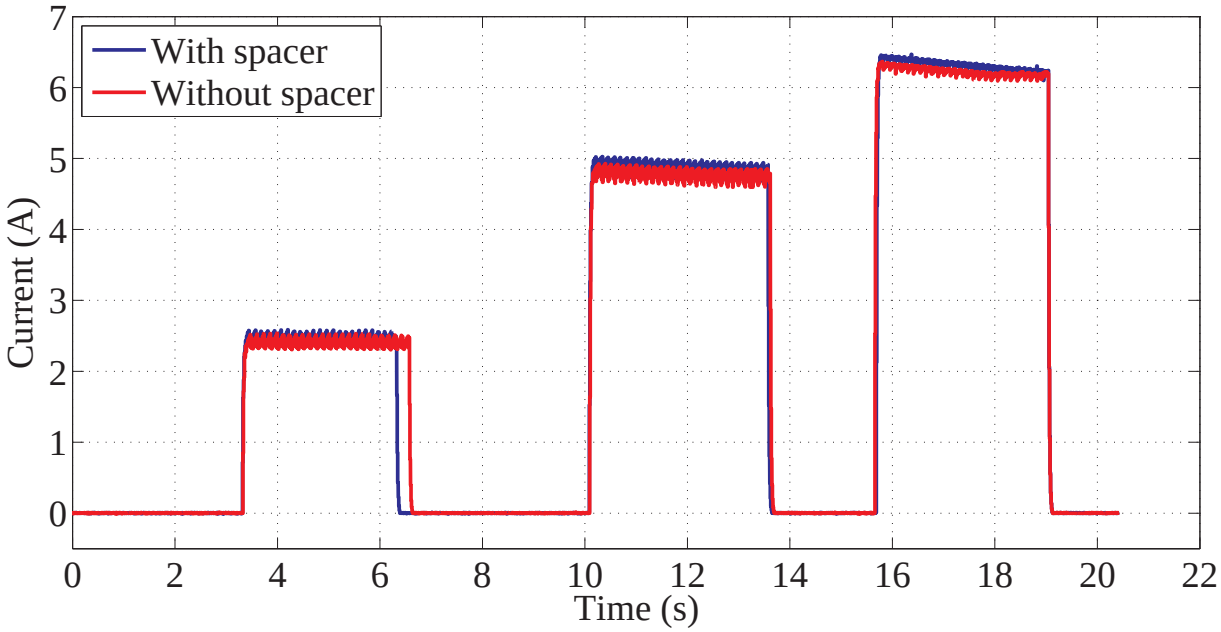

Figure 2.21 Measured current of the actuator with and without the air gap spacer - Air gap length 2.5 *mm*

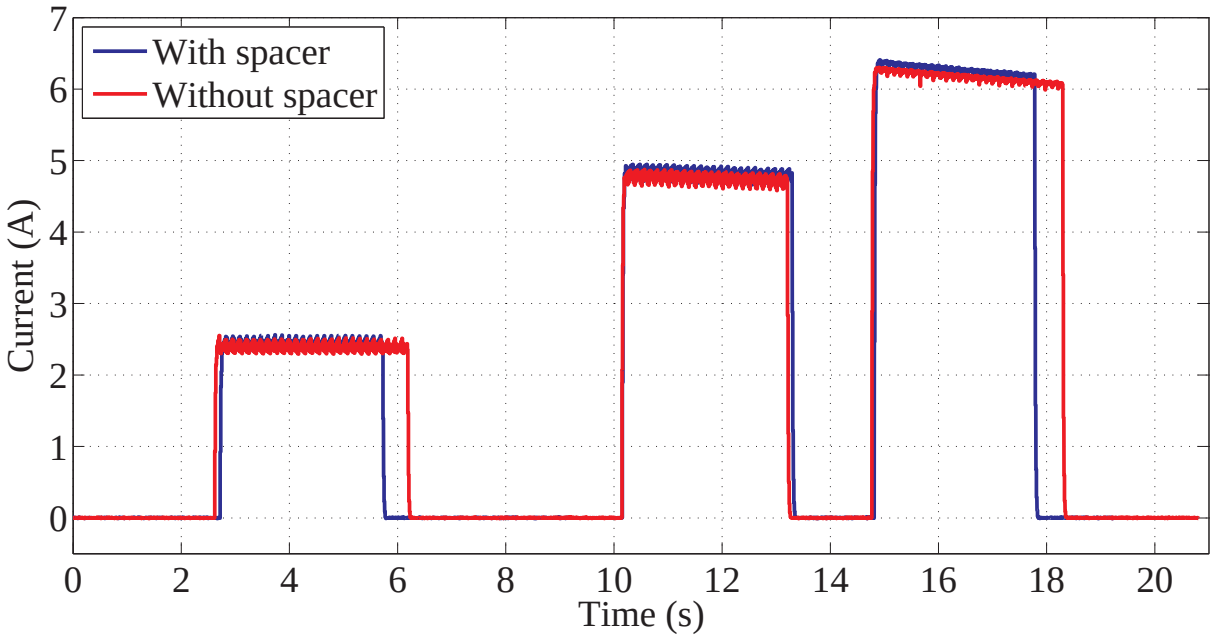

Figure 2.22 Measured current of the actuator with and without the air gap spacer - Air gap length 3.5 *mm*

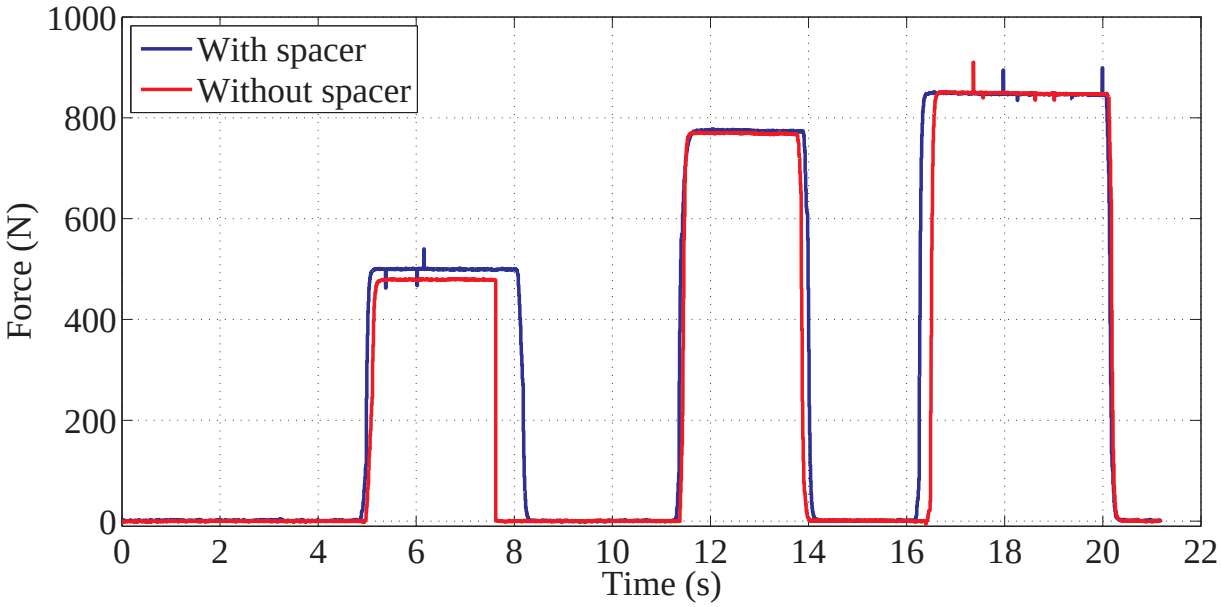

Figure 2.23 Measured force of the actuator with and without the air gap spacer - Air gap length 0.5 *mm*

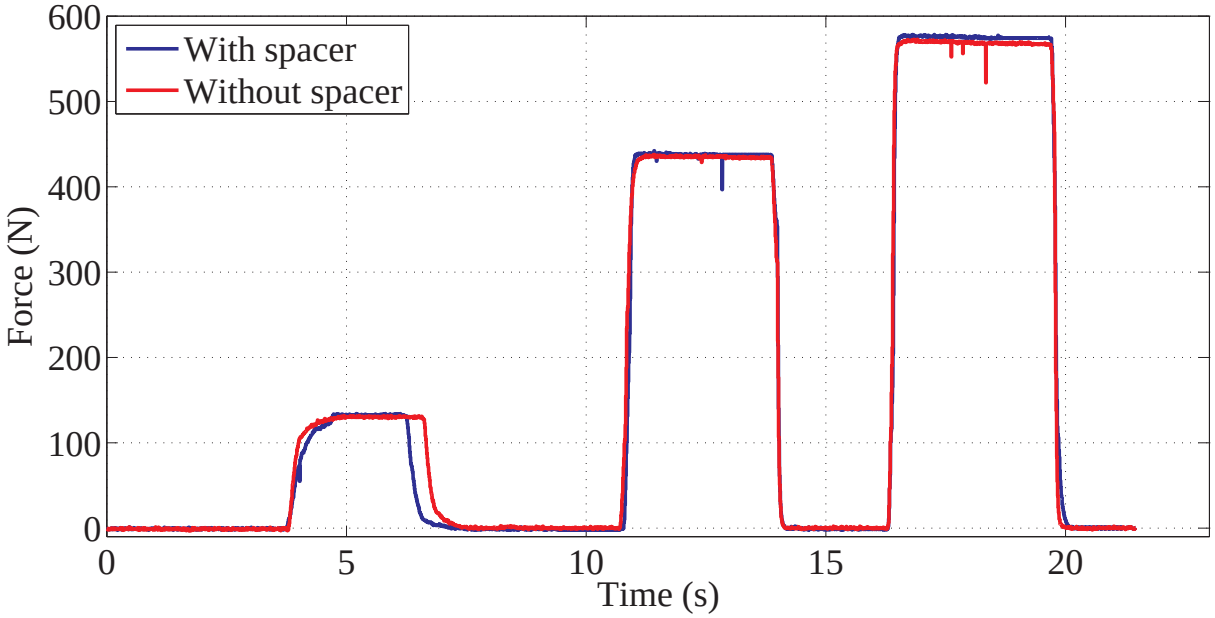

Figure 2.24 Measured force of the actuator with and without the air gap spacer - Air gap length 1.5 *mm*

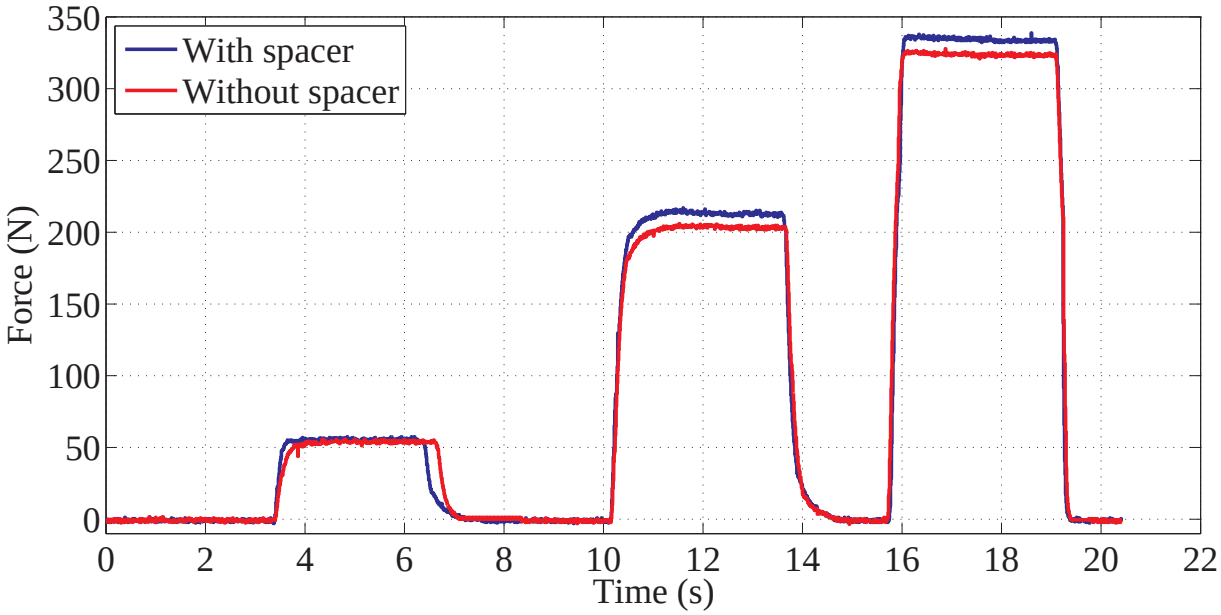

Figure 2.25 Measured force of the actuator with and without the air gap spacer - Air gap length 2.5 *mm*

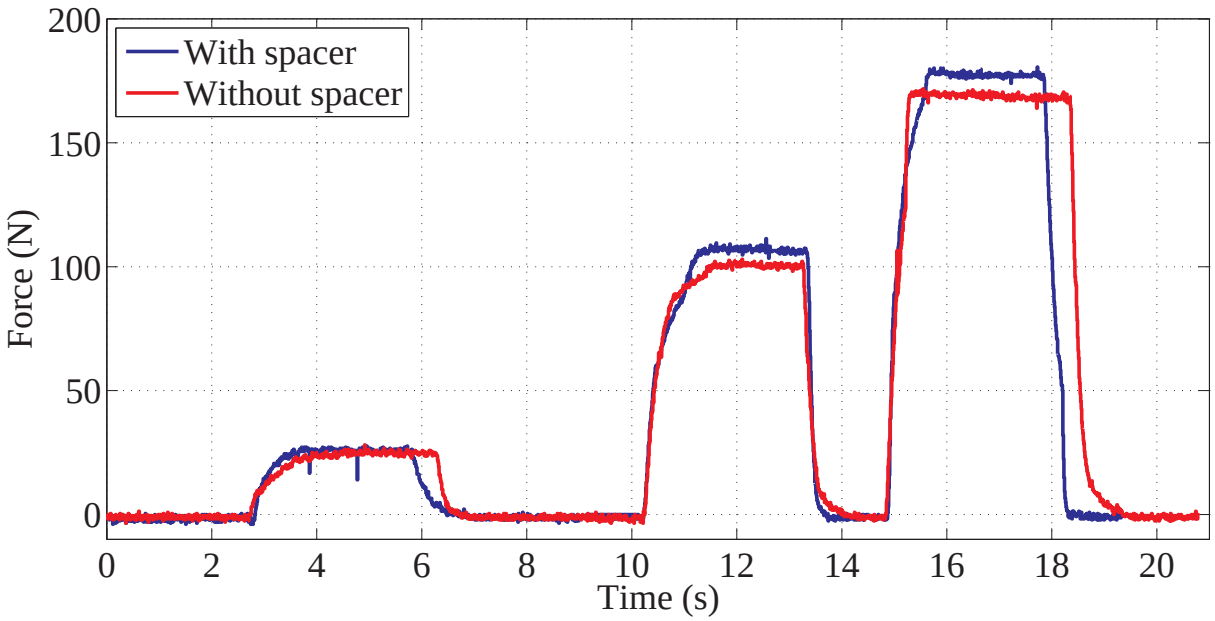

Figure 2.26 Measured force of the actuator with and without the air gap spacer - Air gap length 3.5 *mm*

significantly affected by presence or lack of the spacer. The small amount of mismatch in some cases is due to the measurement errors. These results are expected as in the steady state the inductance of the actuator acts as a short circuit and the resistance of the coil is the only factor in determining the current.

By examining the force graphs, we can see that the generated force is reduced when the spacer is removed. Therefore, the force is more sensitive to the presence of the stainless steel spacer. This is mainly because the total length of the air gap is shorter when the air gap spacer is used and the total reluctance is reduced. Therefore, the presence of the air gap spacer has increased the electromagnetic force in addition to creating a gap between the two ferromagnetic material components.

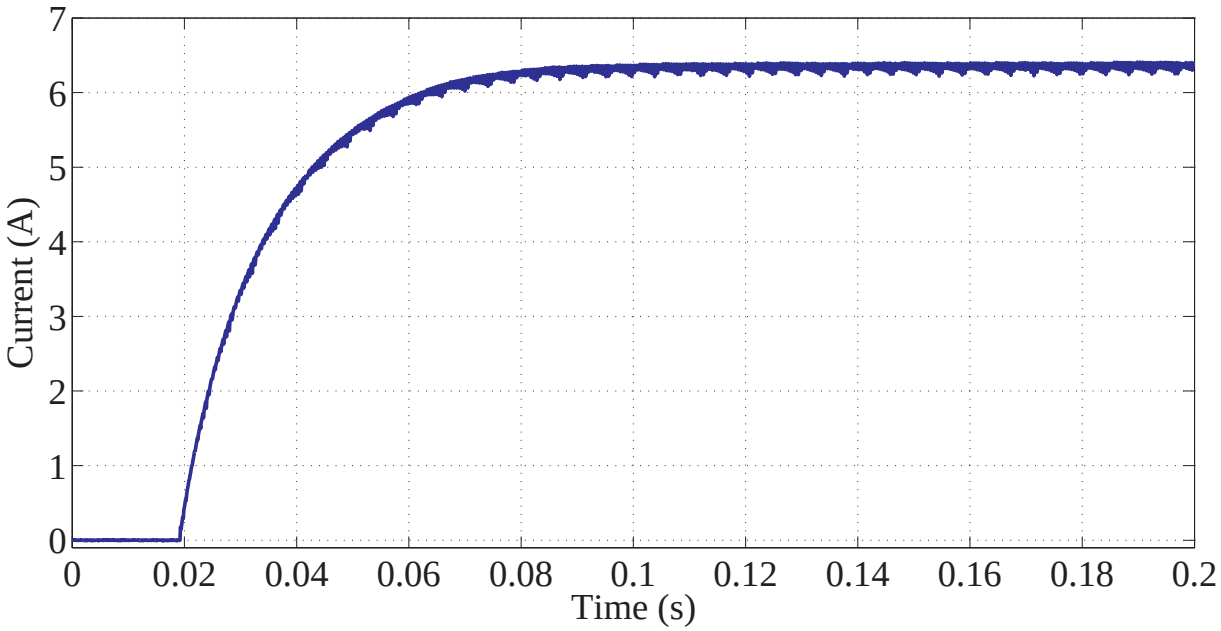

Figure 2.27 Measured output current for input Voltage of 26.7 Volts and 1 mm length of the main air gap

2.2.3.2 Solenoid Actuator Dynamic Modeling

The second main purpose of the experimental tests is analyzing the dynamic behavior of the actuator. The experiments are designed for dynamic system identification of the solenoid actuator. Since the step input covers a wide range of frequencies, the step response will be analyzed for the system identification purpose [49]. Fig. 2.27 shows the measurement noise and PWM effects on the current measurements. In this experiment, a step voltage of 26.7 V at time 0.02 s is applied to the actuator while the main air gap length is 1 mm.

In order to perform the dynamic modeling of the actuator different step voltages (10, 20, and 26.7 Volts) are produced to be applied to the system. To do this, the corresponding DC commands (1.83, 3.64, and 5) are generated by the real time computer and given to the driver. Then, the driver output would be the PWM voltage signals. To find the impact of the main air gap length variations on the dynamics of the system, this test is performed for

different lengths of the main air gap (from 0.5 mm to 1.5 mm in increments of 0.5 mm). The output currents are measured for various input voltages and main air gap lengths. The obtained results for the air gap lengths of 0.5 and 1.5 mm are identical to the results in Figs. 2.19–2.20 when the spacer is retained. For the air gap lengths of 1 mm the current figure is illustrated in Fig. 2.28.

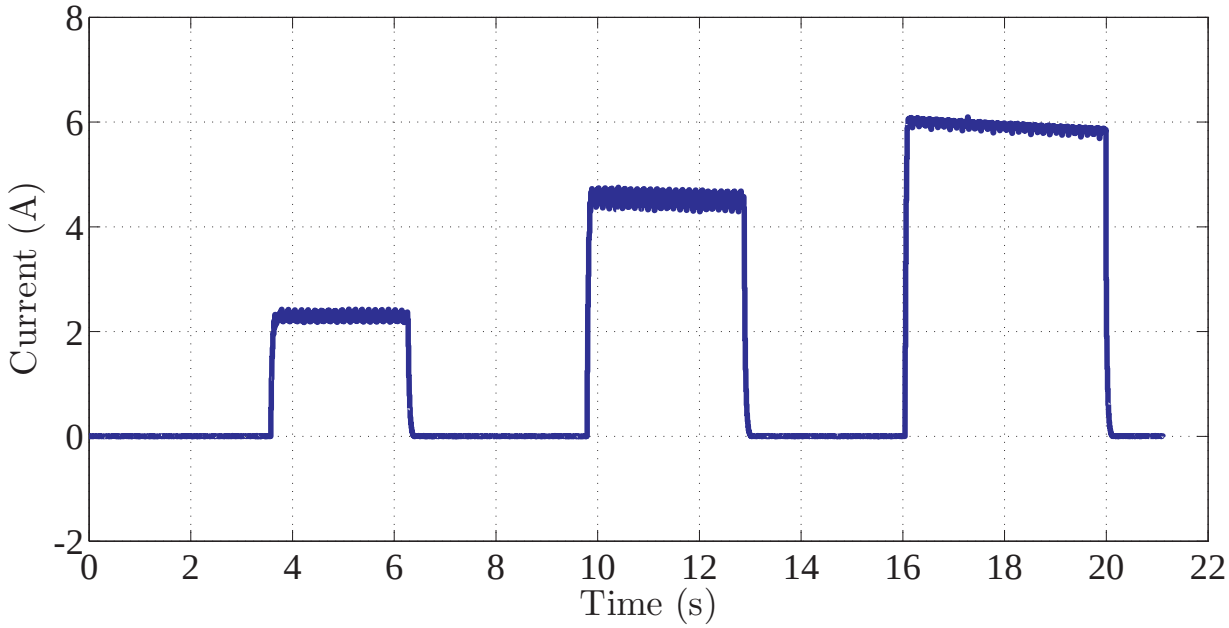

Figure 2.28 Measured current of the actuator - Air gap length 1 mm

2.2.3.3 Experimental Result System Identification

As mentioned earlier in Section 2.2.2, a first order low pass system can describe the electric behavior of the actuator. Using the output current measurement results for each step voltage and main air gap length, a first order system in the Laplace domain is estimated for each case as follows in (2.31).

$$\frac{I}{V} = \frac{k}{s+p} \tag{2.31}$$

The data from experimental results are divided into two sets; one set for the rising of the current after the step voltage is applied and one set for the falling current when the step voltage is going to zero. Three different step voltages are applied to the actuator for three different positions of the plunger and the current is measured in both rising and falling states. Therefore, we have 18 sets of data and system identification process is performed on these sets of data. System identification results are presented in Table 2.4. In this Table the values of k and p are coming from (2.31) where $k = 6.69 \pm \%31$ and $p = 28.5 \pm \%40$. In the system identification of each set of data, instrument variable approach is used. The associated number of iterations, fitting percentage, and final prediction error (FPE) for each set of data is calculated and shown in the table.

The bode magnitude plot of each estimated system is shown in Fig. 2.29. The gray region around the magnitude bode plot is the confidence region. This region indicates that the bode plot of the estimated transfer function will fall within this region. The changes in the magnitude bode plot of estimated systems shows that the temperature rise and plunger displacements were the most significant factors in affecting the electric behavior of the actuator.

Table 2.4 Results of system identification on experimental data

Air gap (mm)	Rising/Falling	Voltage (V)	Iter. #	Syst.	Fitting (%)	FPE
0.5	Rising	10	1	$\frac{4.93}{s+20.58}$	92.36	0.0078
0.5	Falling	10	6	$\frac{5.482}{s+22.19}$	90.79	0.0074
0.5	Rising	20	1	$\frac{6.517}{s+27.09}$	89.01	0.051
0.5	Falling	20	4	$\frac{7.29}{s+30.68}$	90.66	0.045
0.5	Rising	26.7	1	$\frac{6.749}{s+28.68}$	91.83	0.056
0.5	Falling	26.7	4	$\frac{7.25}{s+31.68}$	94.4	0.028
1	Rising	10	1	$\frac{5.81}{s+25.35}$	92.51	0.0067
1	Falling	10	6	$\frac{6.771}{s+29.61}$	94.07	0.0044
1	Rising	20	1	$\frac{5.826}{s+25.28}$	92.07	0.031
1	Falling	20	5	$\frac{7.237}{s+31.92}$	94.21	0.015
1	Rising	26.7	1	$\frac{7.685}{s+34.03}$	93.63	0.033
1	Falling	26.7	5	$\frac{8.755}{s+39.89}$	96.54	0.01
1.5	Rising	10	1	$\frac{6.034}{s+24.9}$	91.97	0.008
1.5	Falling	10	5	$\frac{6.395}{s+26.41}$	92.36	0.008
1.5	Rising	20	1	$\frac{6.952}{s+28.65}$	92.32	0.028
1.5	Falling	20	4	$\frac{6.738}{s+28.044}$	90.96	0.032
1.5	Rising	26.7	1	$\frac{6.799}{s+28.48}$	92.53	0.047
1.5	Falling	26.7	4	$\frac{7.197}{s+29.61}$	94.94	0.024

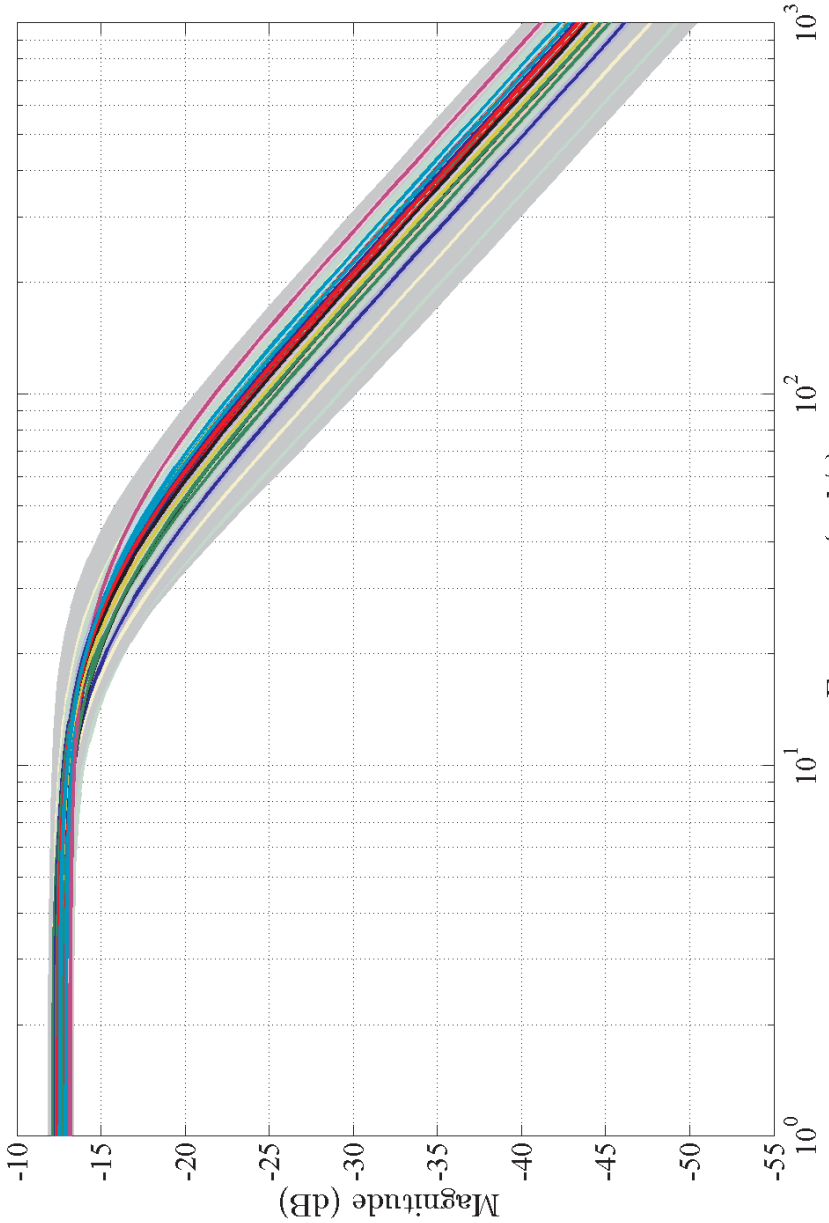

Figure 2.29 Magnitude bode plots of perturbed systems

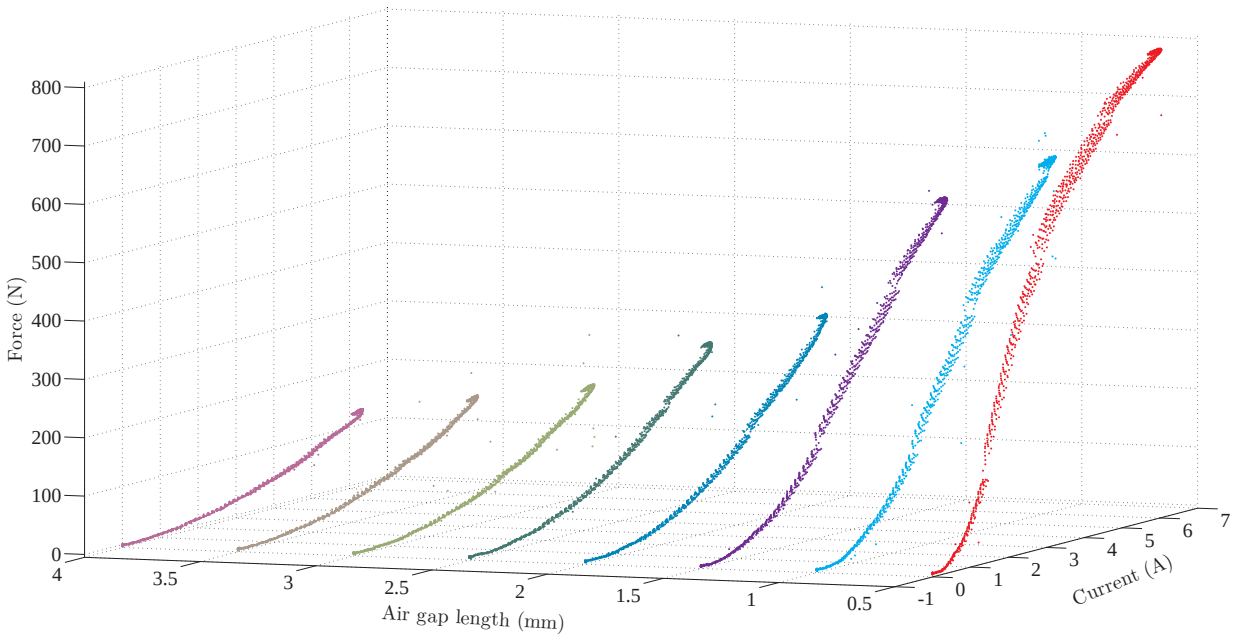

Figure 2.30 Experimental result

2.2.3.4 Solenoid Actuator Static Modeling

In the previous section, current-voltage transfer functions were estimated for different operating conditions. In this section, the purpose of the experimental tests is to find the algebraic relationship between the actuator's main air gap, the input current to the solenoid, and the resulting force. By having this relationship along with the current-voltage transfer function, a reliable model for the actuator can be achieved.

The experimental tests in this section are carried out by applying a ramp voltage from zero to the maximum (26.7 V) to the solenoid actuator. The resulting current and force are measured for different lengths of the main air gap (from 0.5 mm to 4 mm with steps of 0.5 mm). Fig. 2.30 shows the results in the frame of a 3D graph of force vs. the air gap length and current.

It can be seen from Fig. 2.30 that this actuator can generate significantly high forces

when operated in the small enough air gaps. Also, it can be seen that in small air gaps, when the current increases, the actuator refuses to generate the force with the same quadratic order. This happens when the actuator is magnetically saturated and increasing current does not lead to an increase in the amount of force with the same trend as before saturation.

As mentioned in Section 2.2.1, (2.23) is valid when the actuator is operated in the linear region and the saturation effects are ignored. In that equation, the electromagnetic force is proportional to the square of the current. In reality, as observed in Fig. 2.30, the actuator may work in the saturation region especially when the current increases. Thus, in order to have a more accurate model, we augment (2.23) by adding an i^3 term to the numerator to compensate for the saturation effects. Considering this, the resulting force vs. current and air gap relationship would be in the form of (2.32).

$$F_e(x,i) = \frac{a}{(b+cx)^2}(di^2 + ei^3) \tag{2.32}$$

A three-dimensional shaded surface in the form of (2.32) is fitted to the experimental results. The fitted 3D surface along with the experimental results (dotted lines) for various main air gap lengths can be found in Fig. 2.31.

Table 2.5 Coefficients of the Fitted Equation

a	b	c	d	e
39.54	-3.998	-2.565	39.63	-3.858

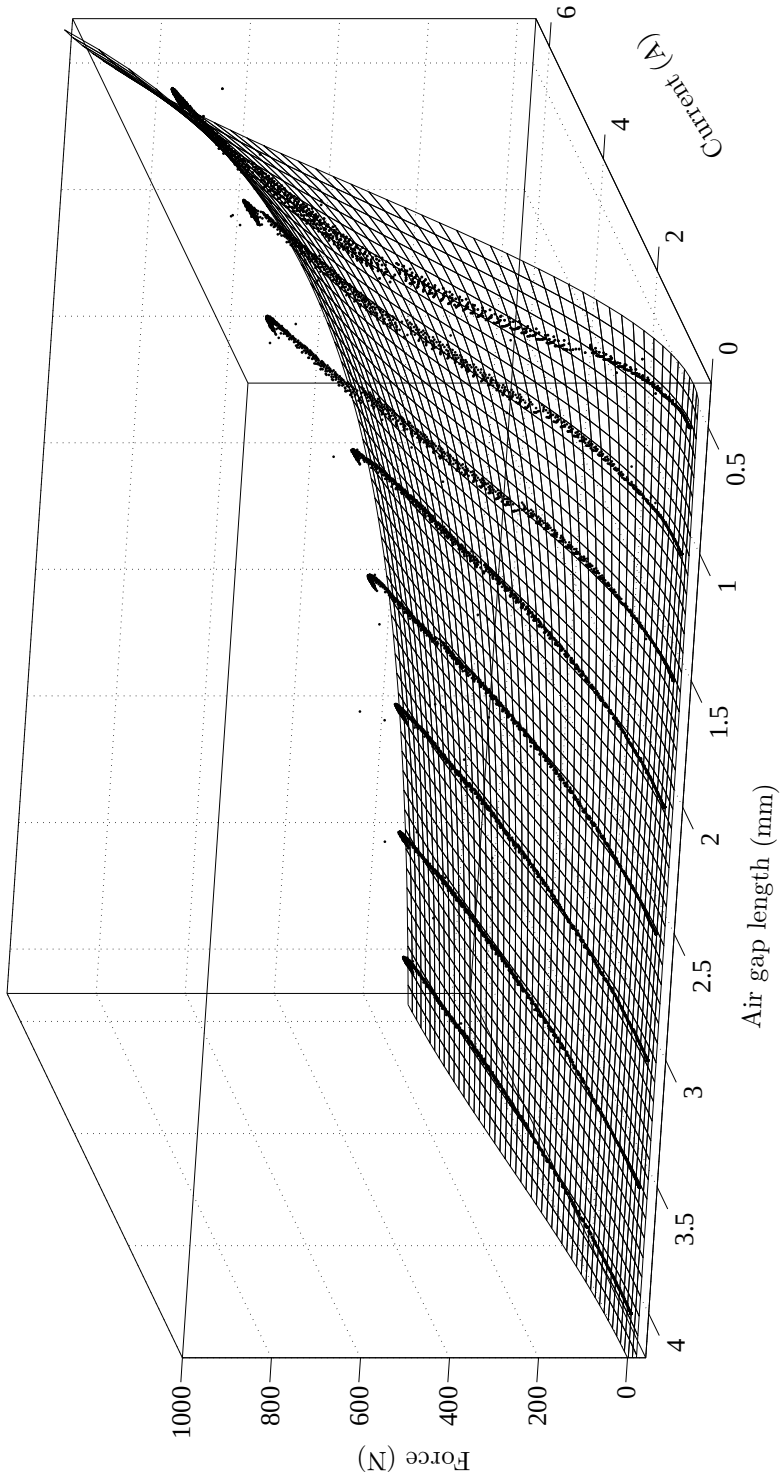

Figure 2.31 3D graph of force versus current and main air gap

The coefficients of (2.32) for fitting the 3D surface seen in Fig. 2.31 are listed in Table 2.5 for the force expressed in Newtons, the current in Amperes, and the air gap in millimeters. According to the above table, the coefficient d is much greater than e. It confirms that the term di^2 is the dominant term and ei^3 can be taken into considerations when the input current increases. Also, the negative sign of e constrains the quadratic current increase and therefore models the impact of magnetic field saturation. The term ei^3 reduces the effective current of the solenoid especially in high currents, which represents the saturation effects in the magnetic field.

Chapter 3

Analysis and Control

As mentioned in the preceding chapters, it is necessary to control the actuator performance to improve the quality of gear shifting in the transmission system of an EV. This chapter is mainly concerned with analyzing the feasibility and design of a closed-loop system to satisfy the stability and performance objectives.

In Chapter 2, the solenoid actuator has been modeled for different operating conditions. We saw that the developed force model as a function of air gap length and current is accurate. However, as Table 2.4 shows, the current-voltage model changes for different values of the excitation voltage and the plunger position.

In this chapter, we first introduce a representative model of uncertainties involved in the modeling of the actuator. This model is essential to control the performance of the actuator. Later, using the model of uncertainties, we will be able to design a robust controller. After implementation of the robust controller, the controller should be able to guarantee the stability and the desired performance of the closed-loop system under realization of any of the uncertainties in their pre-defined range. When the robust controller is designed, the robust performance and stability of the closed-loop system for all the uncertain plants are

verified and the results are presented.

3.1 Uncertainty Analysis

In this section, the uncertainty of the parameters which directly influence the system dynamics are taken into account. In Chapter 2, we saw that the main parameters affecting the performance of the actuator were the resistance of the coil and the main air gap length.

Resistance of the coil is sensitive to the temperature rise. Also, the errors involved in measuring this parameter, would influence on its uncertainty level. The coil temperature and consequently the coil resistance are affected by the actuator's steady state operation [50, 51]. As observed in Chapter 2, the resistor's temperature rise was 31°C when the supplied voltage was 26.7 V and the actuator was under operation for about four seconds. Assuming the initial temperature was at 25°C, the coil temperature had reached to 56 °C. Accordingly, the coil resistance has varied as much as 12% around its nominal value. The nominal value of the resistance is $R = 3.7\ \Omega$ which is the coil resistance at the room temperature.

The air gap length is affected by the measurement errors, as well. Furthermore, it is subject to change as a result of the ambient vibrations. Also, the elastic deformation of the fixture elements would be another reason for the plunger's position uncertainty. Since we require the plunger to produce high forces for a better gear shifting, the nominal air gap length should be selected accordingly. The maximum force corresponds to the maximum driving voltage at the shortest air gap between the plunger and the core (see Fig. 2.4 and Fig. 2.30). Considering this, the nominal air gap length is selected to be 1 mm. Also, the main air gap length is considered to be uncertain as much as 50%.

In addition to the above mentioned uncertainty sources, there are some uncertainties

associated with the deviation of each perturbed plant from its estimated transfer function which are caused by the system identification process. In other words, as a result of system identification of any data, no transfer function can absolutely be fitted for a set of data. Fig. 2.15 and Fig. 2.29 shows that there is a confidence region around each bode plot which guarantees that the transfer function of the data would certainly fall in that region. Such uncertainties could influence the robustness of the controller as well.

The uncertainty model of the solenoid actuator can be obtained by considering the parametric uncertainty involved in the dynamics of the system. Owing to the similar behavior of the perturbed systems (uncertain systems) shown in Fig. 2.29, the uncertainty is represented by considering the additive uncertainty model as expressed in (3.1).

$$G_p = G + W_a\Delta, \quad \|\Delta\|_\infty < 1 \tag{3.1}$$

where G and G_p are the nominal and perturbed systems, respectively. Δ represents a perturbation in the set of all norm-bounded stable additive uncertainties. W_a is the additive uncertainty weighting function which represents the uncertainty model of present system. The weighting function W_a must be selected in a way to cover all the perturbations from the nominal plant, *i.e.* $G_p - G$, in the frequency domain.

In this study, the uncertain systems which include the parametric uncertainty, are the ones derived from experimental tests. The nominal system, with no parametric uncertainty, is derived from the FEM results. The obtained W_a in the Laplace domain is as follows

$$W_a = \frac{3.518s + 25.58}{s^2 + 56.22s + 755.1} \tag{3.2}$$

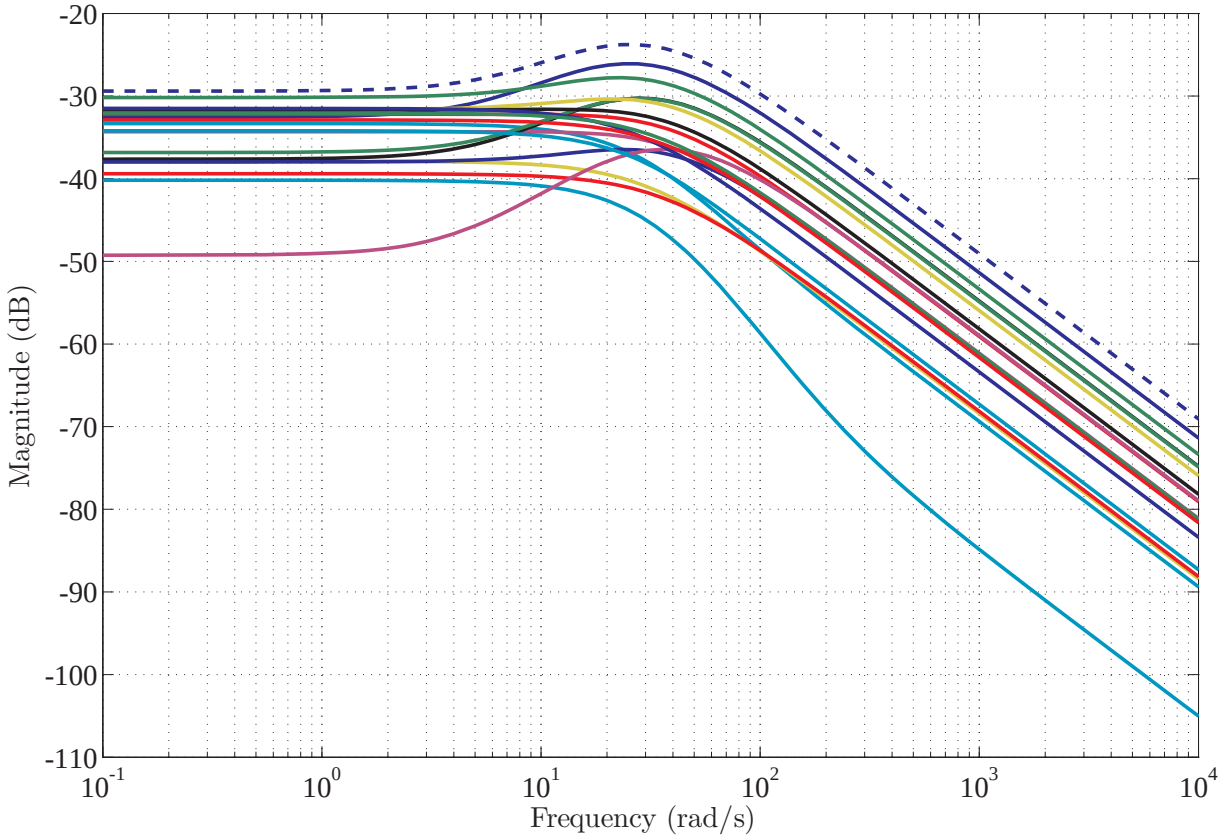

Figure 3.1 Magnitude bode plot of additive weighting function (dashed line) and perturbations of the nominal plant

The magnitude bode plot of perturbations of the uncertain systems from the nominal system, $(G_p - G)$, along with the additive weighting function W_a, the dashed line, are illustrated in Fig. 3.1. As the figure shows, the weighting function, W_a, properly covers all the perturbations. Moreover, W_a is selected conservatively by assuming a confidence gap between the perturbations and the weighting function.

The achieved weighting function, W_a, representing all the possible uncertainties enables us to proceed to design a closed-loop system capable of taking care of all perturbed plants.

3.2 Controller Design

Designing a robust controller would provide not only the closed-loop robustness against the uncertainties, but also a desirable performance for the closed-loop system.

3.2.1 Closed-loop system configuration

As was discussed in Section 2.2, the models representing the actuator's behavior are developed using various approaches. According to (2.27) and (2.31), the relationship between current and excitation voltage is a *linear dynamic* relationship which is represented by a first order transfer function. Nevertheless, the relationship between the electromagnetic force and the current is a *nonlinear algebraic* relationship and there is no dynamic between the two signals, see equation 2.32. Considering the algebraic relationship between the force and the current of the actuator, a new closed-loop control strategy is selected in this thesis which is based on decomposing the actuator's model into a nonlinear algebraic part and a linear dynamic part. Such decomposition leads to the following subsystems

1. Nonlinear force to current algebraic subsystem: this subsystem is basically the inverse of the relationship between force and current presented in (2.32). Such nonlinear inverse relationship can be represented by a lookup table to provide the required current for the desired known force and air gap. In other words, the force and air gap are the inputs to the aforementioned lookup table where the output is the corresponding current that can generate such a force.

2. Linear dynamic current to voltage subsystem: this subsystem is essentially using the models derived from equations (2.27) and (2.31). The dynamic behavior of this part of the system is the result of parameter p in (2.31), discussed in Chapter 2. The purpose of the present closed-loop robust control approach is controlling the current

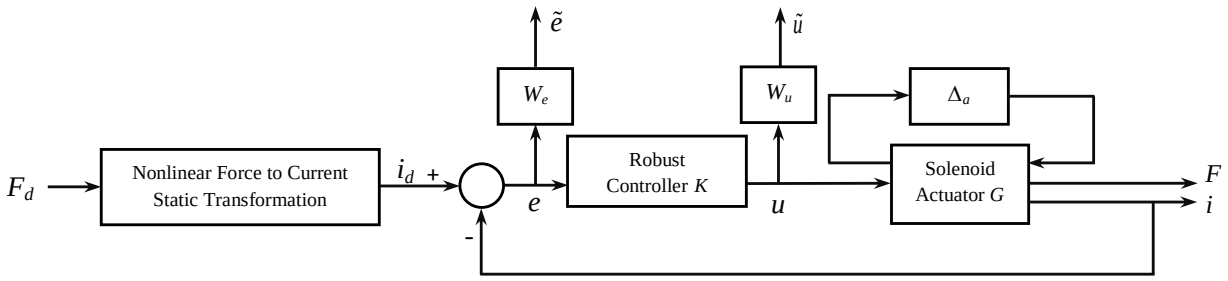

Figure 3.2 Closed-loop system block diagram

of the actuator in a closed-loop configuration to satisfy the desired robustness and performance objectives.

The above mentioned decomposition strategy transforms the closed-loop control problem from the nonlinear force control problem into a linear current control problem. Removing the non-linearity from the control loop substantially reduces the complexity of the closed-loop control system.

3.2.2 H_∞ optimal control

Block diagram of the closed-loop system is shown in Fig. 3.2. The desired closed-loop system output i_d (the corresponding current of the desired force F_d from the first subsystem) is fed to the closed-loop system and the system's outputs are F and i (controlled force and current). The controller's output is the required input voltage, u.

The performance objectives are defined by W_e and W_u where the performance weighting function W_e is the weighting function on the error signal (e) to limit the error at low frequencies. W_u is the weighting function on the control signal (u) constraining the controller's output. The closed-loop performance of the system is also measured by the

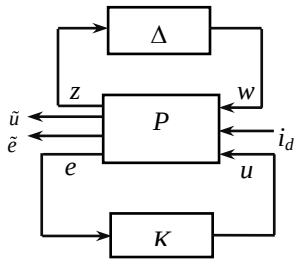

Figure 3.3 Standard LFT diagram for H_∞ optimal control design

normalized parameters $\tilde{u}$ and $\tilde{e}$. In Fig. 3.2, the actuator's uncertainty is Δ_a where

$$\Delta_a = W_a \Delta, \quad \|\Delta\|_\infty < 1 \tag{3.3}$$

The robust controller is designed by solving an optimization problem using the H_∞ optimal control method. This type of optimal control method is concerned with designing a controller which can attenuate the disturbance and meet the desired performance. So, H_∞ control tries to decrease the sensitivity of a system to the disturbance [52]. To do so, the closed-loop system is recast as a linear fractional transformation (LFT), as can be seen in Fig. 3.3. In this figure, P is the generalized plant. Inspection of Fig. 3.2 and Fig. 3.3 shows that

$$\begin{bmatrix} z \\ \tilde{u} \\ \tilde{e} \\ e \end{bmatrix} = \begin{bmatrix} 0 & 0 & W_a \\ 0 & 0 & W_u \\ -W_e & W_e & -GW_e \\ -1 & 1 & -G \end{bmatrix} \begin{bmatrix} w \\ y_d \\ u \end{bmatrix} \tag{3.4}$$

Once the closed-loop system is rearranged in the standard LFT form, the optimization

problem is to find an appropriate stabilizing controller K,

$$\min_{K stabilizing} \|T_{zw}\|_\infty \tag{3.5}$$

where T_{zw} is the closed-loop transfer matrix from the uncertainty output w to the uncertainty input z (see Fig. 3.3). If P is written in the partitioned form

$$P = \begin{bmatrix} P_{11,(3\times2)} & P_{12,(3\times1)} \\ P_{21,(1\times2)} & P_{22,(1\times1)} \end{bmatrix} \tag{3.6}$$

Then,

$$T_{zw} = P_{11} + P_{12}K(I - P_{22}K)^{-1}P_{21} \tag{3.7}$$

Using the small gain theorem [53], for all $\Delta \in RH_\infty$ and $\|\Delta\|_\infty < 1$, the closed-loop system is well-posed and internally stable if and only if $\|T_{zw}\|_\infty < 1$. Hence, the controller K should be found such that $\|T_{zw}\|_\infty$ remains less than one.

Appropriate weighting functions W_e and W_u are chosen as follows

$$W_e = \frac{250}{5s+1} \tag{3.8}$$

$$W_u = \frac{0.0167(0.1s+1)}{0.01s+1} \tag{3.9}$$

Applying the H_∞ optimal control method to our closed-loop system results in a controller which provides the desirable performance as well as the robustness. For the selected weighting functions, the following fifth order H_∞ optimal controller is obtained, *i.e.* the

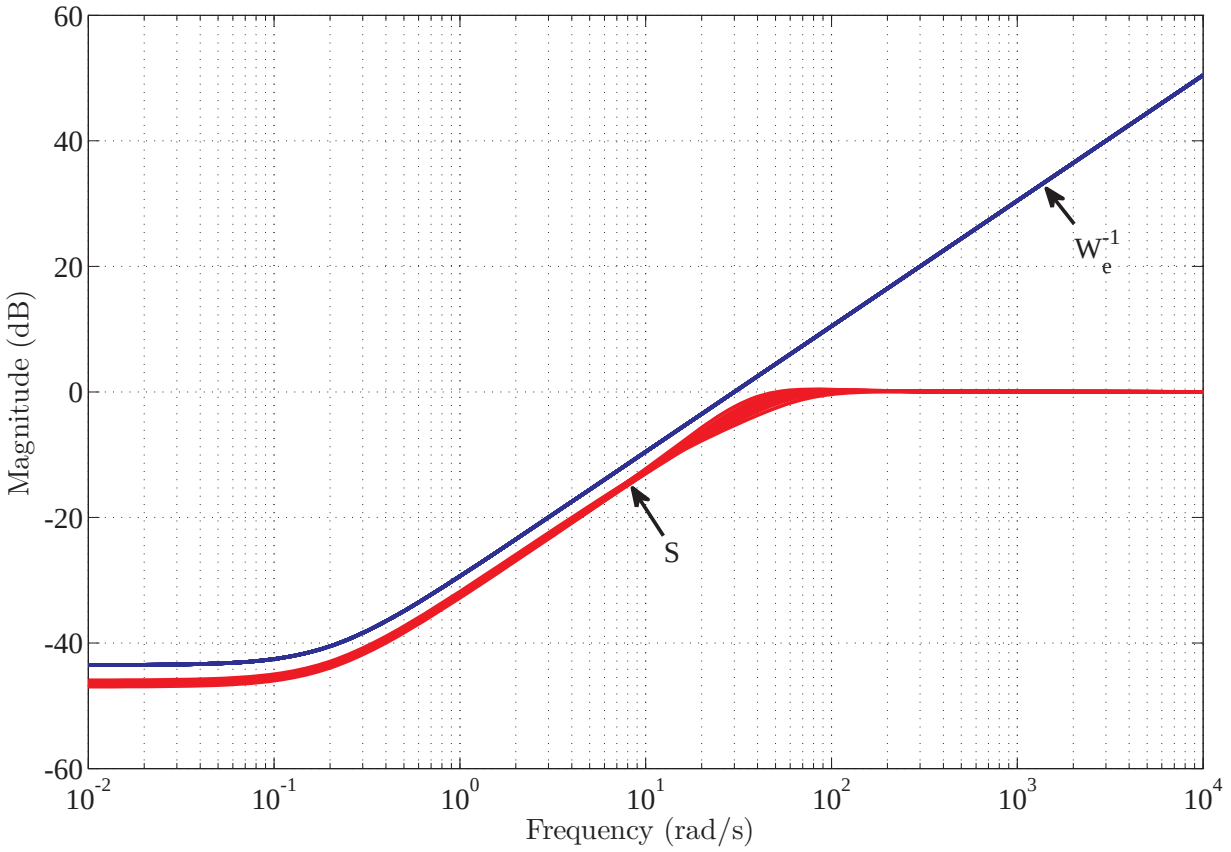

Figure 3.4 Magnitude bode plot pf the nominal and perturbed plants sensitivity along with W_e^{-1}

controller that can achieve $\|T_{zw}\|_\infty < 1$.

$$K = \frac{2.549 \times 10^4 s^4 + 4.76 \times 10^6 s^3 + 2.842 \times 10^8 s^2 + 6.891 \times 10^9 s + 5.881 \times 10^{10}}{s^5 + 6030 s^4 + 7.374 \times 10^5 s^3 + 2.797 \times 10^7 s^2 + 3.327 \times 10^8 s + 6.543 \times 10^7} \quad (3.10)$$

The corresponding $\|T_{zw}\|_\infty$ is 0.3273 . To ensure that stability and performance objectives are met for all the nominal and perturbed plants, the magnitude bode plot of sensitivity of all the plants along with the inverse of the error weighting function (W_e^{-1}) is illustrated in Fig. 3.4.

It can be observed that the bode plot of all the nominal and perturbed plants' sensitivities are below the bode plot of W_e^{-1}. This confirms that robust stability and performance criteria are achieved. To further visualize whether the robust performance is satisfied, the closed-loop system simulation results are presented in the next section.

3.3 Simulation results

In order to validate the performance of the controller in the closed-loop configuration, time domain simulations are performed. The performance objectives are selected as follows:

- Settling time should be less than 0.1 seconds.
- The supply voltage should not exceed 33 Volts. The risk of damaging the actuator will increase as the voltage crosses the 33 Volts limit.
- The output force should be 500 N. This force is sufficient for the gear shifting process.

To verify that the H_∞ optimal controller provides desirable performance, the closed-loop control system is simulated using the nominal system (from FEM approach) as well as the perturbed systems (from the experimental approach). The desired input is a step function with the final value of 500 N and the step time of 0.1 s. The simulation results are shown in Figs. 3.5–3.7. It can be seen that for all system uncertainties, the closed-loop system remains stable, which indicates the robust stability. Moreover, the voltage and force figures confirm that the desirable performance objectives have been met which indicates the robust performance.

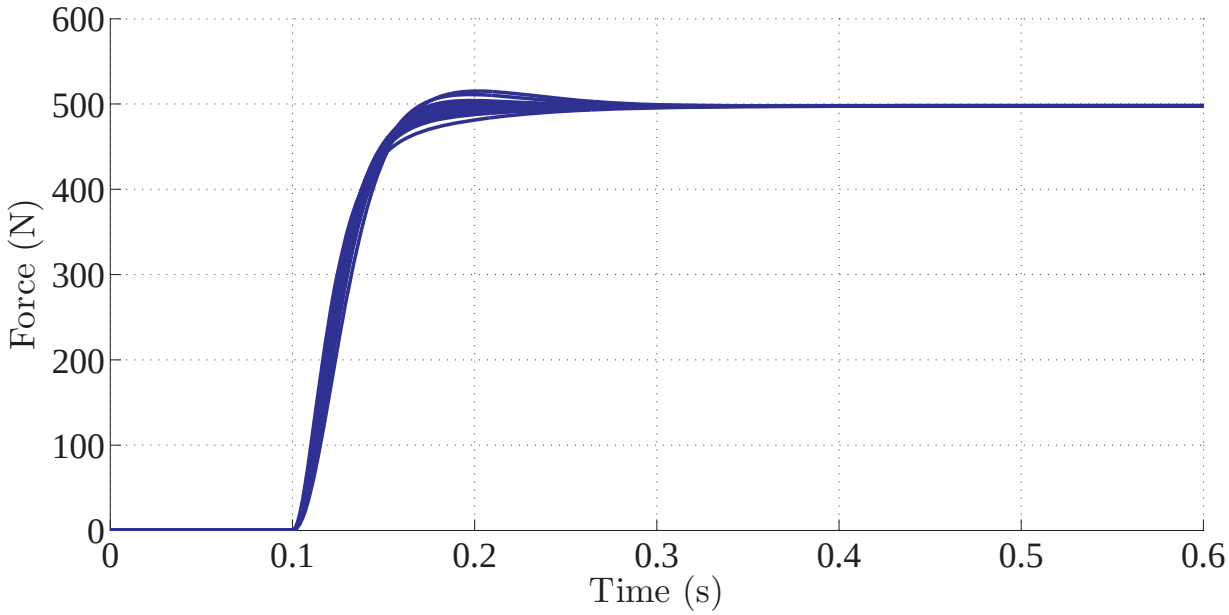

Figure 3.5 Closed-loop system force of all perturbed systems

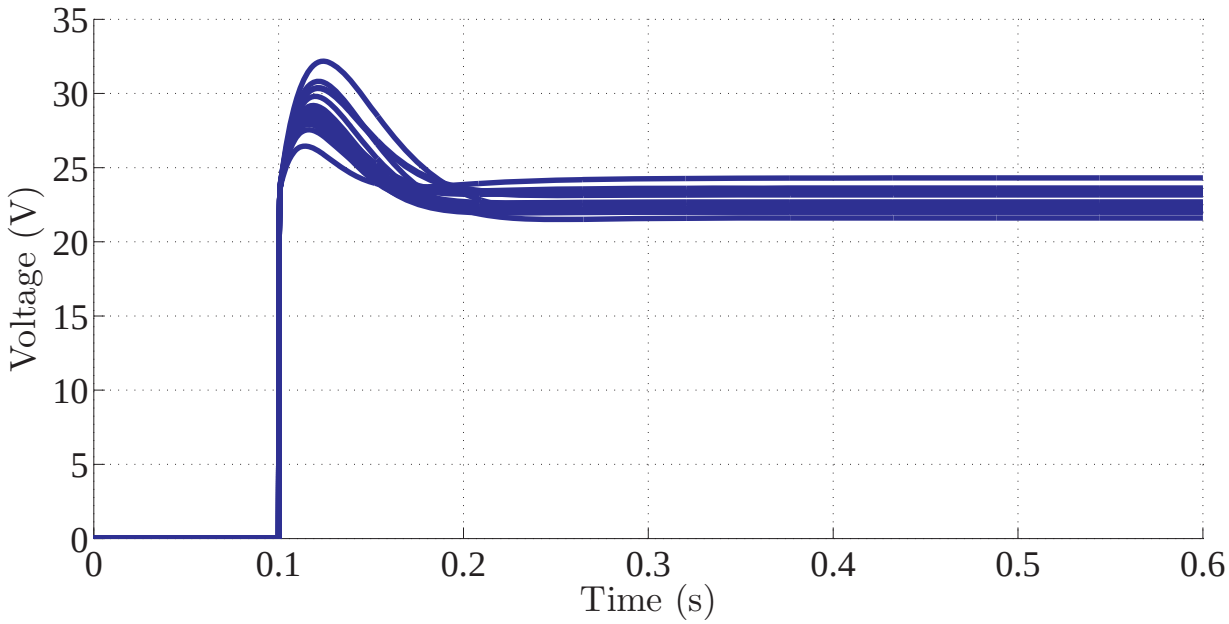

Figure 3.6 Closed-loop system voltage of nominal and perturbed systems

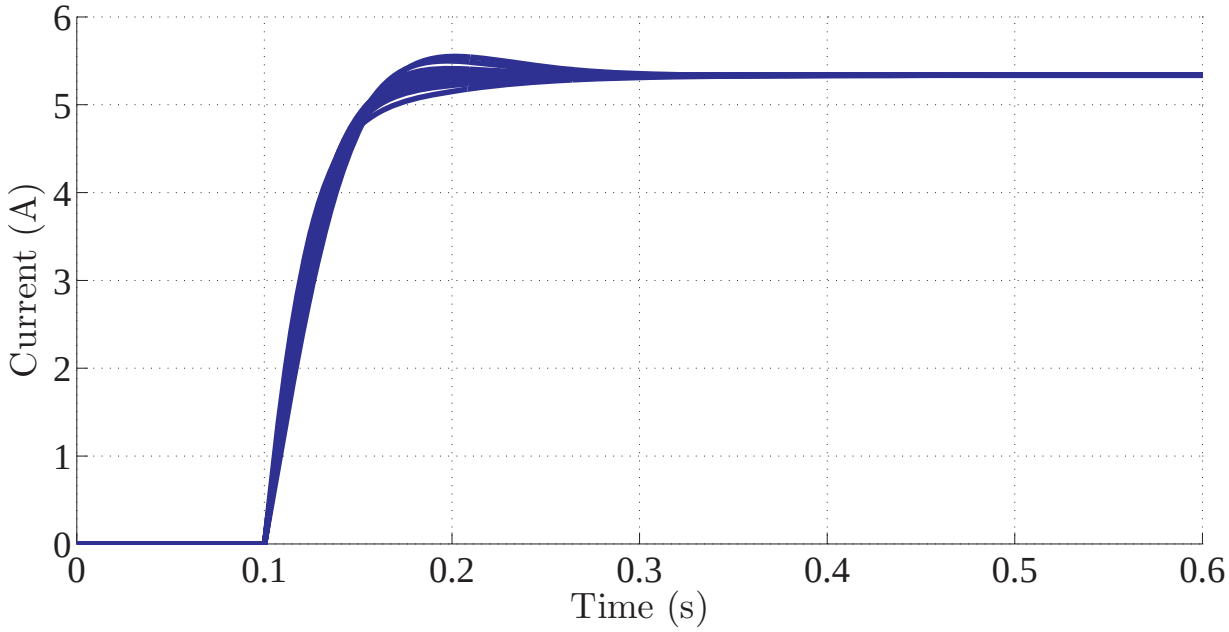

Figure 3.7 Closed-loop system current of nominal and perturbed systems

Chapter 4

Conclusion and Future Work

4.1 Summary

Air pollution as an environmental concern has received a lot of attention in the recent decades. ICEVs are one of the main contributors to the emission of green house gases to the atmosphere. EVs are considered as an alternative to the conventional ICEVs. Various types of transmission systems can modulate the flow of energy from the electric motor to the wheels. The transmission systems have their own advantages and disadvantages. AMT is a type of transmission system which is designed to benefit from the advantages of both manual and automatic transmission systems. Gear shifting in this type of transmission is executed using an actuator. Several types of actuators have been deployed so far to perform gear shifting. Solenoid actuator is considered as an alternative to the conventional hydraulic and electrohydraulic actuators currently being employed in industry. The feasibility of replacing other type of actuators with solenoid actuators in AMTs has been analyzed in this dissertation.

Due to the electromagnetic nature of solenoid actuators, it is not straight forward to

develop a model which describes the behavior of this type of actuator. Maxwell's equations which can describe the electric and magnetic interactions in an electromagnetic device are hard to solve. To have a reliable model of the actuator, several approaches have been introduced in this study. Assuming that the ferromagnetic materials in the actuator do not saturate, a simplified theoretical approach is described. The developed model is not accurate since saturation effects are not considered. The second approach to the modeling of the actuator is based on finite element analysis. FEM is able to take into account the saturation effects. However, there are some parameter variations that FEM does not consider in its calculations. The complementary approach to the modeling is the experimental approach using an experimental setup built to display parameter variation impacts on the actuator's electromagnetic behavior. Using the experimental data collected during the tests, several models of the actuator under various operating conditions are obtained.

To improve the gear shifting quality in an AMT and achieve a smooth shifting experience, the force of the actuator should be controlled in a closed-loop system. Considering the parameter variations in the modeling of the actuator, a robust optimal controller is designed for this type of actuator. The modeling results obtained from FEM and experimental approaches were applied for control purposes. The performance of the robust controller is validated by simulating the closed-loop control of the obtained models from the modeling results. The results show that the controller has achieved the desired performance and robustness.

4.2 Conclusion

The following points are concluded from the results of this work:

a) Due to high density force, low cost, and compact design that solenoid actuators offer,

they are a reasonable option to replace the hydraulic and electro-hydraulic actuators in vehicles equipped with AMT.

b) Since a high amount of force during a short time is desired for the gear shifting in AMT systems, solenoid actuators are a suitable choice when operated in shorter duty cycles. Otherwise, it would damage the actuator's windings.

c) Simplified theoretical equations are derived assuming that the actuator is working in the linear region. Therefore, this approach is not suitable for modeling the actuators working in the saturation region.

d) FEM is a powerful tool in considering not only the geometric and material non-linearities, but also the magnetic field saturation effects. FEM is an alternative to the theoretical approach.

e) FEM is not capable of analyzing the impacts of changes in the key parameters. The solenoid actuator model is found to be sensitive to the variations of parameters such as the temperature and the plunger's position. Experimental approach is the complementary approach selected for modeling.

f) Existence of the air gap spacer had no significant impact on the amount of current in the steady state operation, even though the force of the actuator was affected by the removal of the spacer. That was mainly due to the increase in the air gap length with the spacer removal.

g) Due to the sources of uncertainties involved in the modeling of the actuator, a robust optimal controller is the best option for controlling the actuator.

h) Transferring the force control problem to the current control problem has removed the nonlinearities from the closed loop system. This is accomplished by a look-up table finding the corresponding current for a desired force at a specified air gap length.

4.3 Future work

The work presented in this thesis can be further expanded as follows:

a) In this study, the usefulness of the closed-loop force control of the actuator in obtaining the desired stability and performance is investigated using simulation. Experimental closed-loop control would be a valuable future work. This will assure the automotive industry that the application of solenoid actuator in the gear shifting of the AMT is indeed beneficial in comparison to the other actuators.

b) In order to improve the gear shifting quality and to have smoother gear shifting experience, the simultaneous control of force and speed would be beneficial in terms of improving the gear shifting quality. The safe seating control will increase the life time of the actuator and will enhance the comfort of the passengers.

c) In order to include the temperature variations in the FEM modeling of the actuator, solving the electromagnetic and thermal fields simultaneously is recommended. This will provide us with a precise FEM model of the actuator.

References

[1] K. Chau and Y. Wong, "Overview of power management in hybrid electric vehicles," *Energy Conversion and Management*, vol. 43, no. 15, pp. 1953–1968, 2002.

[2] C. Chan, "The rise & fall of electric vehicles in 1828–1930: Lessons learned [scanning our past]," *Proceedings of the IEEE*, vol. 101, no. 1, pp. 206–212, 2013.

[3] U. Eberle and R. von Helmolt, "Sustainable transportation based on electric vehicle concepts: a brief overview," *Energy & Environmental Science*, vol. 3, no. 6, pp. 689–699, 2010.

[4] T. Wiedmann and J. Minx, "A definition of 'carbon footprint'," *Ecological economics research trends*, vol. 1, pp. 1–11, 2008.

[5] L. Lu, X. Han, J. Li, J. Hua, and M. Ouyang, "A review on the key issues for lithium-ion battery management in electric vehicles," *Journal of Power Sources*, vol. 226, pp. 272–288, 2013.

[6] R. Heath and A. Child, "Zeroshift automated manual transmission (AMT)," SAE Technical Paper, Tech. Rep., 2007.

[7] M. Kulkarni, T. Shim, and Y. Zhang, "Shift dynamics and control of dual-clutch transmissions," *Mechanism and Machine Theory*, vol. 42, no. 2, pp. 168–182, 2007.

[8] R. Toom, "Les boites de vitesses automobiles," in *CTI seminar*, 2006.

[9] G. Wagner, "Application of transmission systems for different driveline configurations in passenger cars," SAE Technical Paper, Tech. Rep., 2001.

[10] M. A. Kluger and D. M. Long, "An overview of current automatic, manual and continuously variable transmission efficiencies and their projected future improvements," SAE Technical Paper, Tech. Rep., 1999.

[11] A. Turner, K. Ramsay, R. Clark, and D. Howe, "Direct-drive rotary-linear electromechanical actuation system for control of gearshifts in automated transmissions," in *Vehicle Power and Propulsion Conference, 2007. VPPC 2007. IEEE.* IEEE, 2007, pp. 267–272.

[12] (2014, Oct.) Manual transmission. [Online]. Available: http://dfwtransmissions.bmbnow.com/

[13] (2014, Oct.) Automatic transmission. [Online]. Available: http://goo.gl/G9Jzmv

[14] G. Lucente, M. Montanari, and C. Rossi, "Modelling of an automated manual transmission system," *Mechatronics*, vol. 17, no. 2, pp. 73–91, 2007.

[15] J. C. Wheals, C. Crewe, M. Ramsbottom, S. Rook, and M. Westby, "Automated manual transmissions-a european survey and proposed quality shift metrics," SAE Technical Paper, Tech. Rep., 2002.

[16] O. Gomis-Bellmunt and L. F. Campanile, *Design rules for actuators in active mechanical systems*. Springer, 2010.

[17] A. Poole and J. D. Booker, "Classification and selection of actuator technologies with consideration of stimuli generation," in *The 15th International Symposium on: Smart Structures and Materials & Nondestructive Evaluation and Health Monitoring*. International Society for Optics and Photonics, 2008, pp. 692 728–692 728.

[18] M. Zupan, M. F. Ashby, and N. A. Fleck, "Actuator classification and selection—the development of a database," *Advanced engineering materials*, vol. 4, no. 12, pp. 933–940, 2002.

[19] A. R. Turner, K. Clark, and D. R Howe, "Direct-drive electromechanical linear actuator for shift-by-wire control of an automated transmission." Vehicle Power and Propulsion Conference, 2006. VPPC'06. IEEE, 2006.

[20] Y. Kawase and Y. Ohdachi, "Dynamic analysis of automotive solenoid valve using finite element method," *Magnetics, IEEE Transactions on*, vol. 27, no. 5, pp. 3939–3942, 1991.

[21] F. Bayat, A. F. Tehrani, and M. Danesh, "Finite element analysis of proportional solenoid characteristics in hydraulic valves," *International Journal of Automotive Technology*, vol. 13, no. 5, pp. 809–816, 2012.

[22] Q. H. Yuan and P. Y. Li, "Self-calibration of push-pull solenoid actuators in electro-hydraulic valves," in *ASME 2004 International Mechanical Engineering Congress and Exposition*. American Society of Mechanical Engineers, 2004, pp. 269–275.

[23] B. Lequesne, "Fast-acting, long-stroke solenoids with two springs," *Industry Applications, IEEE Transactions on*, vol. 26, no. 5, pp. 848–856, 1990.

[24] N. Vaughan and J. Gamble, "The modeling and simulation of a proportional solenoid valve," *Journal of dynamic systems, measurement, and control*, vol. 118, no. 1, pp. 120–125, 1996.

[25] L. Cao, S. Mantell, and D. Polla, "Design and simulation of an implantable medical drug delivery system using microelectromechanical systems technology," *Sensors and Actuators A: Physical*, vol. 94, no. 1, pp. 117–125, 2001.

[26] Q. Niu and Y. Liu, "H-infinity control theory in vehicle diesel fuel injection pump control system design," in *Machine Vision and Human-Machine Interface (MVHI), 2010 International Conference on*, April 2010, pp. 98–100.

[27] P. Wellstead and N. Pettit, "Analysis and redesign of an antilock brake system controller," in *Control Theory and Applications, IEE Proceedings-*, vol. 144, no. 5. IET, 1997, pp. 413–426.

[28] C. Stefanini, G. Orlandi, A. Menciassi, Y. Ravier, G. La Spina, S. Grillner, and P. Dario, "A mechanism for biomimetic actuation in lamprey-like robots," in *Biomedical Robotics and Biomechatronics, 2006. BioRob 2006. The First IEEE/RAS-EMBS International Conference on*. IEEE, 2006, pp. 579–584.

[29] K. Ogata, *System dynamics*. Pearson/Prentice Hall, 2004, vol. 13.

[30] P. Prest and N. Vaughan, "Drive circuits for pulse width modulated valves," in *Proc. International conference on fluid power, March*, 1987, pp. 24–26.

[31] S. Yamada, Y. Kanamaru, and K. Bessho, "The transient magnetization process and operations in the plunger type electromagnet," *Magnetics, IEEE Transactions on*, vol. 12, no. 6, pp. 1056–1058, 1976.

[32] M. Fauri and P. Sonato, "A finite element analysis of an electromagnetic flow control valve," *Magnetics, IEEE Transactions on*, vol. 27, no. 5, pp. 3912–3915, 1991.

[33] B. P. Lequesne, "Finite-element analysis of a constant-force solenoid for fluid flow control," *Industry Applications, IEEE Transactions on*, vol. 24, no. 4, pp. 574–581, 1988.

[34] S. Butzmann, J. Melbert, and A. Koch, "Sensorless control of electromagnetic actuators for variable valve train," *Training*, vol. 2013, pp. 12–05, 2000.

[35] M. F. Rahman, N. C. Cheung, and K. W. Lim, "Position estimation in solenoid actuators," *Industry Applications, IEEE Transactions on*, vol. 32, no. 3, pp. 552–559, 1996.

[36] P. Eyabi and G. Washington, "Modeling and sensorless estimation for single spring solenoids," *Studies*, vol. 2013, pp. 08–14, 2006.

[37] F. Ronchi, C. Rossi, and A. Tilli, "Sensing device for camless engine electromagnetic actuators," in *IECON 02 [Industrial Electronics Society, IEEE 2002 28th Annual Conference of the]*, vol. 2. IEEE, 2002, pp. 1669–1674.

[38] H. V. Alizadeh and B. Boulet, "Robust control of synchromesh friction in an electric vehicle's clutchless automated manual transmission," in *Control Applications (CCA), 2014 IEEE Conference on*. IEEE, 2014, pp. 611–616.

[39] H. V. Alizadeh, M. Helwa, and B. Boulet, "Constrained control of the synchromesh operating state in an electric vehicle's clutchless automated manual transmission," in *Control Applications (CCA), 2014 IEEE Conference on*. IEEE, 2014, pp. 623–628.

[40] L. Lovas, D. Play, J. Marialigeti, and J.-F. Rigal, "Mechanical behaviour simulation for synchromesh mechanism improvements," *Proceedings of the Institution of Mechanical Engineers, Part D: Journal of Automobile Engineering*, vol. 220, no. 7, pp. 919–945, 2006.

[41] (2014, Oct.) Low profile actuator. [Online]. Available: http://www.ledex.com/ltr2/access.php?file=pdf/LowProfile_Section.pdf

[42] R. M. Bozorth, "Ferromagnetism," *Ferromagnetism, by Richard M. Bozorth, pp. 992. ISBN 0-7803-1032-2. Wiley-VCH, August 1993.*, vol. 1, 1993.

[43] S. E. Lyshevski, *Electromechanical systems, electric machines, and applied mechatronics*. CRC press, 1999, vol. 3.

[44] G. Dhatt, E. Lefrançois, and G. Touzot, *Finite element method*. John Wiley & Sons, 2012.

[45] R. Tahmasebi, H. V. Alizadeh, S. Rahimi, and B. Boulet, "Robust h_∞ force control of a solenoid actuator using experimental data and finite element method," in *Control Applications (CCA), 2014 IEEE Conference on*. IEEE, 2014, pp. 1172–1177.

[46] J. Webb and B. Forghani, "T-omega method using hierarchal edge elements," *IEEE Proceedings-Science, Measurement and Technology*, vol. 142, no. 2, pp. 133–141, 1995.

[47] ——, "Dc current distributions and magnetic fields using the t-omega edge-element method," *Magnetics, IEEE Transactions on*, vol. 31, no. 3, pp. 1444–1447, 1995.

[48] P. C. Young, "An instrumental variable method for real-time identification of a noisy process," *Automatica*, vol. 6, no. 2, pp. 271–287, 1970.

[49] S. Ahmed, B. Huang, and S. L. Shah, "Novel identification method from step response," *Control Engineering Practice*, vol. 15, no. 5, pp. 545–556, 2007.

[50] S. J. Domanski, "Effects contributing to the temperature rise of electromagnetic actuators," *Development*, vol. 2009, pp. 03–01, 2000.

[51] H. Mizutani, Y. Noda, T. Miyoshi, K. Terashima, M. Nishida, and N. Suganuma, "Robust rebound suppression control for push-pull solenoid considering the characteristic change during operation," in *SICE Annual Conference 2010, Proceedings of*. IEEE, 2010, pp. 137–143.

[52] S. Skogestad and I. Postlethwaite, *Multivariable feedback control: analysis and design*. Wiley New York, 2007, vol. 2.

[53] K. Zhou, J. C. Doyle, K. Glover *et al.*, *Robust and optimal control*. Prentice Hall New Jersey, 1996, vol. 272.